© 2022. Published by The Company of Biologists Ltd | Journal of Cell Science (2022) 135, jcs259374. doi:10.1242/jcs.259374

RESEARCH ARTICLE

MTCL2 promotes asymmetric microtubule organization by crosslinking microtubules on the Golgi membrane

Risa Matsuoka*, Masateru Miki*, Sonoko Mizuno, Yurina Ito, Chihiro Yamada and Atsushi Suzuki‡

ABSTRACT

The Golgi complex plays an active role in organizing asymmetric microtubule arrays, which are essential for polarized vesicle transport. The coiled-coil protein MTCL1 stabilizes microtubules nucleated from the Golgi membrane. Here, we report an MTCL1 paralog, MTCL2, which preferentially acts on the perinuclear microtubules accumulated around the Golgi. MTCL2 associates with the Golgi membrane through the N-terminal coiled-coil region and directly binds microtubules through the conserved C-terminal domain without promoting microtubule stabilization. Knockdown of MTCL2 significantly impaired microtubule accumulation around the Golgi, as well as the compactness of the Golgi ribbon assembly structure. Given that MTCL2 forms parallel oligomers through homo-interaction of the central coiled-coil motifs, our results indicate that MTCL2 promotes asymmetric microtubule organization by crosslinking microtubules on the Golgi membrane. Results of *in vitro* wound healing assays further suggest that this function of MTCL2 enables integration of the centrosomal and Golgi-associated microtubules on the Golgi membrane, supporting directional migration. Additionally, the results demonstrated the involvement of CLASPs and giantin in mediating the Golgi association of MTCL2.

KEY WORDS: MTCL1, MTCL2, SOGA, SOGA1, Golgi ribbon, Microtubules, Polarity

INTRODUCTION

The microtubule (MT) cytoskeleton plays an essential role in organizing intracellular structures by mediating the transport and positioning of organelles. Generally, animal cells radiate MTs from the centrosome, where MT nucleation and attachment of MT minus ends predominantly occur (Conduit et al., 2015; Vorobjev and Nadezhdina, 1987). However, accumulating evidence has demonstrated that cultured cells also develop non-centrosomal MTs that nucleate from or attach their minus ends to the Golgi membrane (Efimov et al., 2007; Meiring et al., 2020; Nishita et al., 2017; Rivero et al., 2009; Wu et al., 2016). In contrast to centrosomal MTs, which exhibit dynamic instability at their plus ends, Golgi-associated MTs are specifically stabilized (Bartolini and Gundersen, 2006; Chabin-Brion et al., 2001; Rivero et al., 2009) and connect the individual Golgi stacks laterally (Miller et al., 2009). This connection leads to the formation of the vertebrate-specific crescent-like assembly of Golgi stacks, called the Golgi ribbon (Miller et al., 2009), which is required for the polarization of vesicle transport and directional migration (Miller et al., 2009; Wei and Seemann, 2010; Yadav et al., 2009).

The molecular mechanisms that mediate the development of Golgi-associated MTs have been studied extensively. Cytoplasmic linker-associated proteins (CLASPs) and AKAP450 promote microtubule nucleation from the Golgi membrane, whereas calmodulin-regulated spectrin-associated proteins (CAMSAPs) are involved in the attachment of MT minus ends to the Golgi membrane (Efimov et al., 2007; Rivero et al., 2009; Sanders and Kaverina, 2015; Wu and Akhmanova, 2017; Wu et al., 2016; Yang et al., 2017). Until recently, however, the stabilization mechanism of Golgi-associated MTs was not well clarified. We previously identified a novel MT-regulating protein named microtubule crosslinking factor 1 (MTCL1) that specifically condenses to the Golgi membrane through the interaction with CLASPs and AKAP450 (Sato et al., 2013, 2014). MTCL1 is a long coiled-coil protein with two MT-binding domains (MTBDs) at the N- and C-terminal regions (Fig. 1A), the latter of which has a unique ability to stabilize the polymerization state of MTs (Abdul Kader et al., 2017; Sato et al., 2013, 2014). By associating with the Golgi membrane, MTCL1 plays an essential role in the stabilization of Golgi-associated MTs through this C-terminal MTBD (C-MTBD) activity. In addition, we also demonstrated that MTCL1 forms parallel dimers via the coiled-coil-rich region and crosslinks Golgi-associated MTs through the N-terminal MTBD (N-MTBD), which lacks MT-stabilizing activity (Abdul Kader et al., 2017).

Invertebrate genomes do not encode proteins homologous to MTCL1, indicating that the above functions of MTCL1 are specifically utilized in vertebrates. By contrast, a single paralog of MTCL1, which we named MTCL2, is encoded in vertebrate genomes. The deduced amino acid sequence of MTCL2 showed significant identity and similarity with MTCL1 in the coiled-coil region and the C-MTBD but not in the N-MTBD (Fig. 1A; Fig. S1). This result suggests that vertebrates exploit other MT-regulating proteins with similar, but not identical, activity to that of MTCL1. However, contrary to this prediction, previous papers have already reported a shorter isoform of mouse MTCL2 lacking the 203 N-terminal amino acids acts as a suppressor of glucose from autophagy (SOGA) with completely different functions from those of MTCL1 (Fig. 1A) (Combs and Marliss, 2014; Cowerd et al., 2010). According to these papers, SOGA (now called SOGA1) is translated as a membrane-spanning protein and is cleaved into two halves at the endoplasmic reticulum (ER) of hepatocytes (Cowerd et al., 2010). The resultant N-terminal fragment is released into the cytoplasm to suppress autophagy by interacting with the Atg5–Atg12–Atg16 complex, whereas the C-terminal fragment is secreted after further cleavage (Fig. 1A).

Molecular Cellular Biology Laboratory, Yokohama City University Graduate School of Medical Life Science, 1-7-29 Suehiro-cho, Tsurumi-ku, Yokohama 230-0045, Japan.
*These authors contributed equally to this work

‡Author for correspondence (abell@yokohama-cu.ac.jp)

A.S., 0000-0002-3026-3026

Handling Editor: Michael Way
Received 10 September 2021; Accepted 20 April 2022

Journal of Cell Science (2022) 135, jcs259374. doi:10.1242/jcs.259374

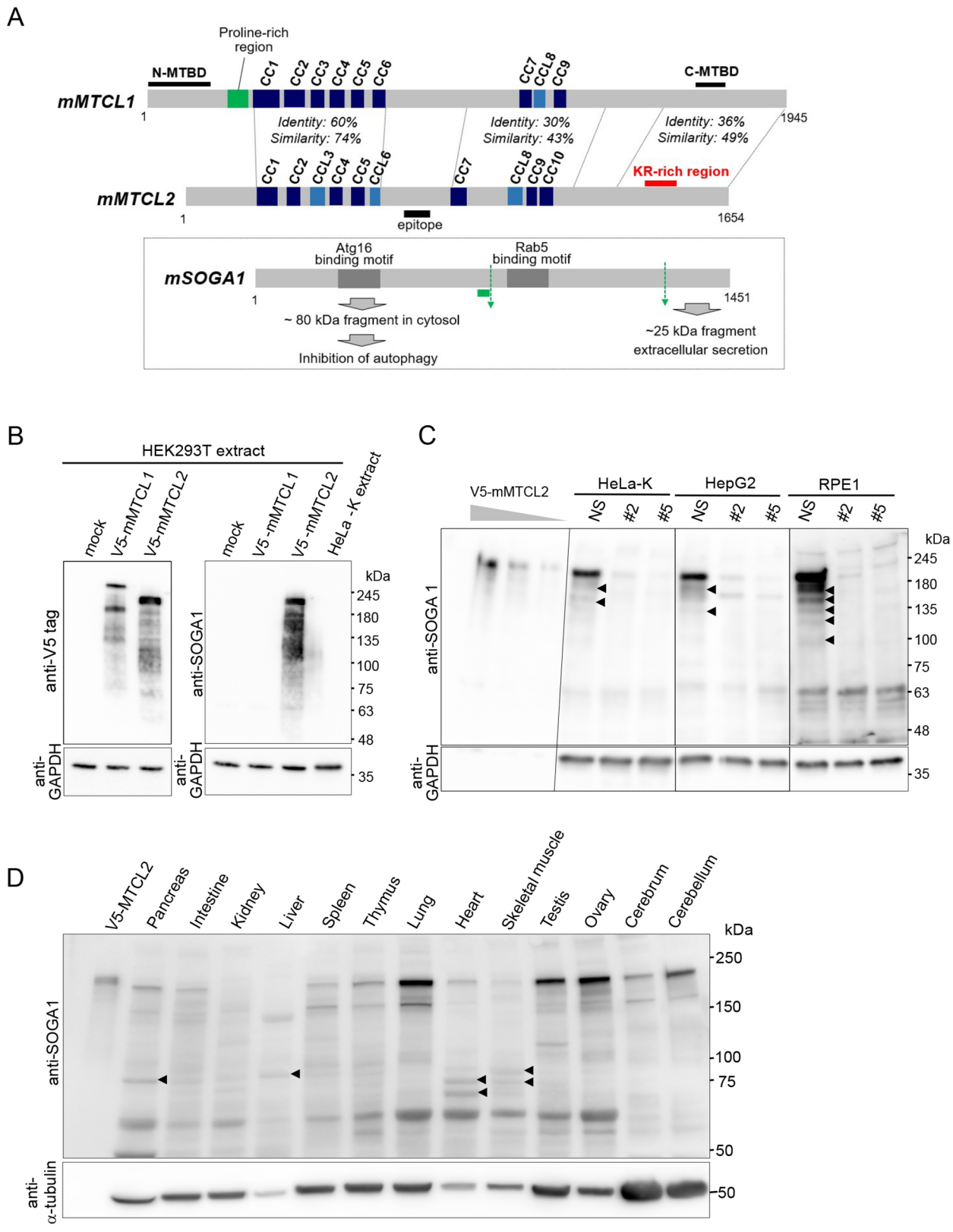

Fig. 1. See next page for legend.

In this study, we first analyzed the expression, subcellular localization and functions of MTCL2, and demonstrate that uncleaved MTCL2 is expressed ubiquitously and functions as a functional paralog of MTCL1 in the cytosol. Structure–function analysis indicated that MTCL1 forms parallel oligomers through the central coiled-coil region and crosslinks MTs by direct interaction via the C-terminal region lacking MT-stabilizing activity. In contrast to MTCL1, the Golgi association region of MTCL2 was

Journal of Cell Science (2022) 135, jcs259374. doi:10.1242/jcs.259374

Fig. 1. MTCL2 is expressed predominantly as a 180 kDa full-length uncleaved protein. (A) Predicted molecular structure of mouse MTCL2 (mMTCL2) (GenBank accession number NM_001164663) and its amino acid sequence similarity and identity with mouse MTCL1 (mMTCL1) (GenBank accession number AK147205). CC (dark blue) corresponds to the region with the highest score (>0.85) of coiled-coil prediction, whereas CCL (light blue) corresponds to the region with a moderate score (>0.4) (Lupas et al., 1991). The black bar labeled 'epitope' indicates the position of the antigen peptide of the anti-SOGA1 antibody used in this study. The red bar indicates the region named the KR-rich region whose amino acid sequence shows significant similarity with C-MTBD of MTCL1 (Fig. S1C). The boxed illustrations at the bottom indicate the structure of mouse SOGA1 (mSOGA1) in comparison with full-length mMTCL2 and summarize the claims presented in the study reporting SOGA1 (Cowherd et al., 2010). The green bar indicates the predicted position of the internal signal sequence, whereas green dotted arrows indicate the predicted positions of cleavages, although we failed to confirm all predictions ourselves. (B) Western blotting analysis of HEK293T extracts transfected with indicated expression vectors. In the mock sample, an empty backbone vector was co-transfected. Antibodies used are indicated on the left of each panel. Note that detection was performed at a low sensitivity, wherein endogenous MTCL2 could not be detected in HEK293T or HeLa-K cell extracts (see lane 1 and 4 in the right panel, respectively). (C) Western blotting analysis of endogenous MTCL2 in various cultured cells using an anti-SOGA1 antibody. In lanes 1–3, cell extracts of HEK293T expressing exogenous V5-mMTCL2 were loaded after serial dilutions (1/10, 1/30 and 1/100). In other lanes, extracts of indicated culture cells with or without MTCL2 knockdown were loaded. NS, non-silencing control; #2 and #5 indicate different siRNAs for MTCL2. (D) Tissue distribution of MTCL2. Total extracts from the indicated mouse tissues (25 µg/lane) were loaded for western blotting analysis using an anti-SOGA1 antibody. In lane 1, total cell extracts of HEK293T expressing exogenously expressed V5-mMTCL2 were loaded as a positive control. Arrowheads in C and D highlight bands with lower molecular mass than that of full-length MTCL2, which disappeared in knockdown conditions. Blots shown are representative of at least two experiments.

distinctly confined to the N-terminal coiled-coil region, which interacted with CLASP2. The involvement of giantin in the Golgi association of MTCL2 has also been suggested. Knockdown experiments revealed that these activities of MTCL2 were required for MT accumulation around the Golgi and the clustering of Golgi stacks into a compact Golgi ribbon. *In vitro* wound-healing assays further suggested a possible function of MTCL2 in integrating the centrosomal and Golgi-associated MTs around the Golgi ribbon, thus playing essential roles in directional migration. These results indicate the important roles of MTCL2 in asymmetrically organizing MTs based on the Golgi complex.

RESULTS

MTCL2 is expressed predominantly as a 180 kDa full-length uncleaved protein

A mouse MTCL2 (mMTCL2) isoform lacking the 203 N-terminal amino acids, named SOGA1, was reported to be cleaved into several fragments on the ER (Fig. 1A) (Cowerd et al., 2010). If this processing occurs for full-length MTCL2, too, it cannot serve as a functional paralog of MTCL1. Thus, we first analyzed the molecular mass of MTCL2 in cultured cells using a commercially available anti-SOGA1 antibody, predicted to detect an ∼80 kDa cleaved product derived from the MTCL2 N-terminus (Fig. 1A). Fig. 1B shows results of western blotting analysis of HEK293T cells transfected with an expression vector harboring full-length mMTCL2 cDNA. Under a low-sensitivity condition at which the anti-SOGA1 antibody revealed no bands in the lanes of untransfected cells (Fig. 1B, right panel; see lanes indicated with 'mock' or 'HeLa-K extract'), a single major band corresponding to a molecular mass of ∼200 kDa was specifically detected in cells expressing exogenous MTCL2 (V5-tagged mMTCL2). This molecular mass is close to the nominal molecular mass of 183,150 kDa predicted for the full-length mMTCL2 product. A similar band was detected using an anti-V5 antibody, indicating that this band corresponds to the major product derived from the transfected cDNA (Fig. 1B, left panel). Reactions with both antibodies yielded additional smeared bands corresponding to molecular masses ranging from 100 to 180 kDa; however, no clear bands ∼80 kDa were detected. Taken together, we conclude that exogenously expressed full-length MTCL2 is not subjected to significant intramolecular cleavage in HEK293T cells.

Next, we examined the molecular mass of endogenous MTCL2 in extracts from several cell lines, including a human liver cancer cell line, HepG2, using the same anti-SOGA1 antibody under higher sensitivity conditions (Fig. 1C). Under these conditions, a major band corresponding to ∼200 kDa was detected in the lanes of HeLa-K, HepG2 and RPE1 cells. These bands corresponded to a molecular mass similar to that of V5–mMTCL2 and were not observed in the lanes of cells subjected to MTCL2 knockdown (Fig. 1C). Considering that the antibody did not cross-react with MTCL1 (Fig. 1B, right panel), these results demonstrate that the examined cell lines predominantly expressed full-length MTCL2. As shown in Fig. 1C, several minor bands corresponding to molecular masses lower than 200 kDa (arrowheads) disappeared in knockdown cells, particularly in RPE1 cells (Fig. 1C). Therefore, they may correspond to splicing isoforms or cleaved products of MTCL2. However, most of the bands corresponded to molecular masses greater than 100 kDa, and clear bands at ∼80 kDa corresponding to an N-terminal cleavage product were not detected. Collectively, these results indicate that endogenous MTCL2 in these cell lines is not subjected to cleavage, which was previously reported for SOGA1 in hepatocytes.

Finally, we performed western blotting analyses of various mouse tissue extracts. The data revealed a ∼200 kDa band in various tissues, especially in the lung, testis, ovary, cerebrum, and cerebellum (Fig. 1D). On the other hand, weak signals at ∼80 kDa were detected for some tissues, such as the pancreas, liver and muscles (arrowheads). These results do not exclude the possibility that MTCL2 is subjected to the reported cleavage and functions in the form of SOGA1 in some tissues. However, the above results are consistent with the notion that MTCL2 is predominantly expressed in the full-length form without cleavage.

MTCL2 intermittently associates with the MT lattice, and preferentially condenses on the perinuclear MTs accumulating around the Golgi complex

Next, we examined the subcellular localization of MTCL2 in HeLa-K cells. The reaction with the anti-SOGA1 antibody yielded granular signals in the cytoplasm, which were particularly condensed near the perinuclear region, where the Golgi ribbons were located and MTs accumulated (top panels in Fig. 2A). These signals disappeared completely in MTCL2-knockdown cells (see Fig. 6), and the same staining patterns were obtained, independent of the fixation conditions (Fig. S2A–D). Therefore, we conclude that the immunostaining signals stained by the anti-SOGA1 antibody reveal the localization of endogenous MTCL2. Close inspection indicated that most MTCL2 signals in the perinuclear region were detected on MTs, and some overlapped with Golgi marker signals (middle panels in Fig. 2A). Colocalization of MTCL2 with MTs was also observed in the peripheral regions, where MTCL2 shows intermittent distribution along MTs as observed for MTCL1 (bottom panels in Fig. 2A,B) (Sato et al., 2013, 2014). The association of MTCL2 with MT was further demonstrated by substantial changes in the MTCL2 signals in

Journal of Cell Science (2022) 135, jcs259374. doi:10.1242/jcs.259374

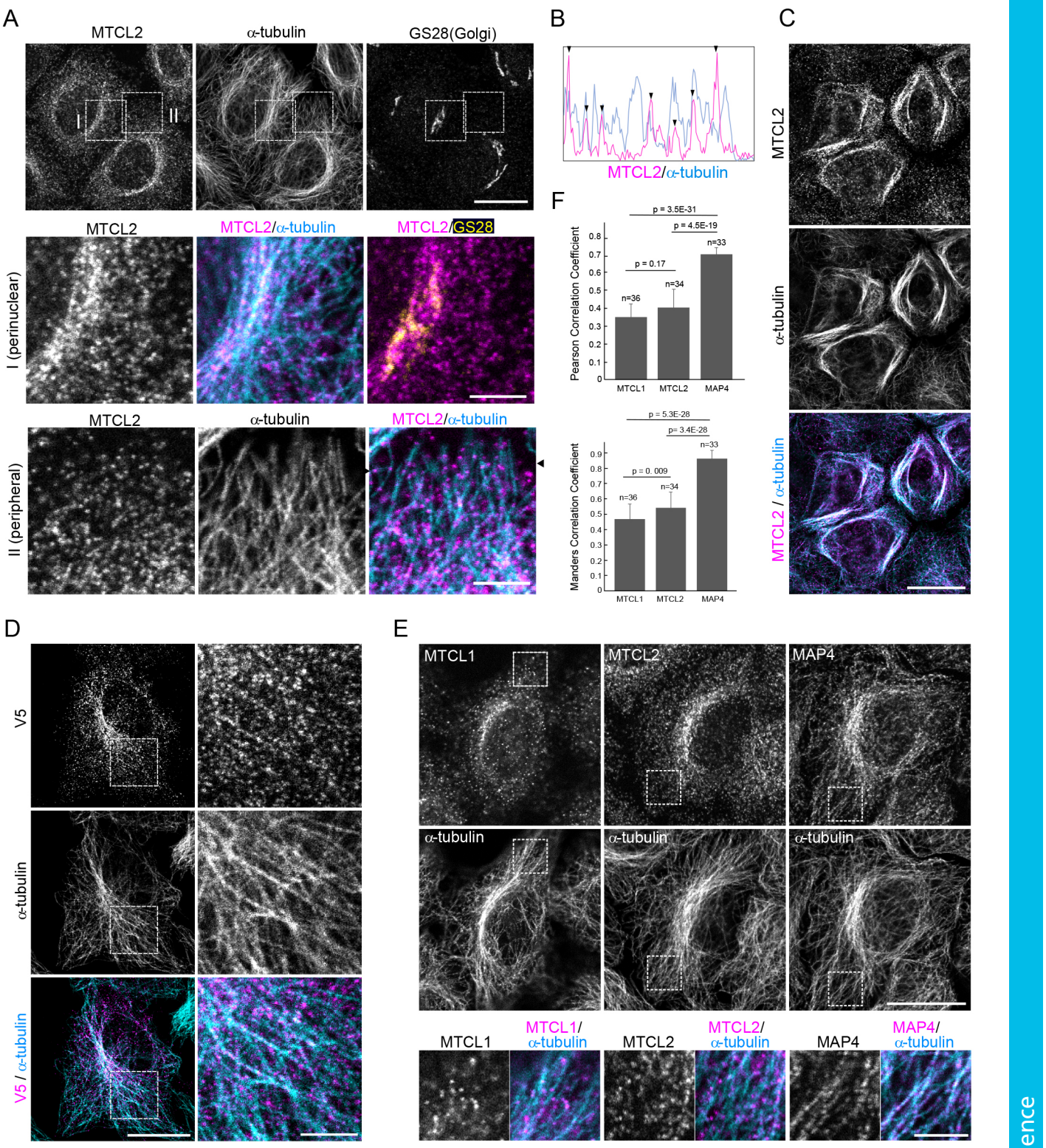

Fig. 2. MTCL2 intermittently associates with the MT lattice, and preferentially condenses on the perinuclear MTs accumulating around the Golgi complex. (A) HeLa-K cells stained with anti-SOGA1 (MTCL2) together with anti-α-tubulin and anti-GS28 antibodies. Scale bar: 20 µm. Boxed regions (I and II) in the top panels are enlarged in middle or bottom panels, respectively. Scale bars: 5 µm. (B) Line scan analysis of immunofluorescence signals of MTCL2 and MTs in the bottom panel in A along a line connecting the red arrowheads. (C) Localization of MTCL2 in cells treated with paclitaxel. (D) Subcellular localization of exogenously expressed V5-tagged MTCL2 in HeLa-K cells analyzed using anti-V5 and anti-α-tubulin antibodies. Scale bar: 20 µm. The boxed region is enlarged in the right panels. Scale bars: 5 µm. (E) HeLa-K cells were stained with anti-MTCL1, SOGA1 (MTCL2), or MAP4 antibodies together with anti-α-tubulin antibody, as indicated. Scale bar: 20 µm. Boxed regions are enlarged in bottom panels. Scale bar: 5 µm. (F) Pearson correlation coefficient (top) and Manders' correlation coefficient (the fraction of MAP signal in pixels containing MT signal; bottom) were calculated for immunofluorescence signals of each the MAPs (MTCL1, MTCL2 and MAP4) and MTs. Data represent the means±s.d. for the indicated number (*n*) of cells from two independent experiments. The *P*-value was estimated using an unpaired Student's *t*-test assuming the two-tailed distribution and two-sample unequal variance. Images shown in A–E are representative of at least two experiments.

Journal of Cell Science (2022) 135, jcs259374. doi:10.1242/jcs.259374

response to paclitaxel treatment. In this condition, most granular MTCL2 signals were concentrated on treatment-induced MT bundles (Fig. 2C).

The MTCL2 distribution patterns observed above were also confirmed for exogenously expressed MTCL2 detected by an anti-tag antibody. When highly expressed in HeLa-K cells, exogenous MTCL2 induced the formation of thick MT bundles to which MTCL2 itself was enriched (arrows in Fig. S2E), and frequently disrupted the typical crescent-like Golgi ribbon structures into dispersed structures (arrows in Fig. S2F). However, cells expressing exogenous MTCL2 at the endogenous levels had the same subcellular localization for MTCL2 as seen for endogenous MTCL2, with it accumulating on one side of the perinuclear region where the Golgi ribbons localize and MTs accumulate (Fig. 2D; Fig. S2E,F). The intermittent localization along peripheral MTs was also confirmed for exogenously expressed MTCL2 detected by the anti-V5 tag antibody (Fig. 2D).

Finally, the subcellular localization of MTCL1 and MTCL2 was compared to another MT lattice-binding protein, microtubule-associated protein 4 (MAP4) (Chapin and Bulinski, 1991). All proteins exhibited preferential condensation to the perinuclear region where MTs are accumulated around the Golgi (Fig. 2E and data not shown). However, in the peripheral regions, distribution patterns of MTCL1 and MTCL2 were significantly different from that of MAP4. MAP4 signals exhibited linear arrangements from which the directions of each MT filament could be predicted. In contrast, the immunofluorescence signals of MTCL1 and MTCL2 were too sparse for such predictions (bottom panels in Fig. 2E). This difference was also validated by a quantitative analysis of MT colocalization for each MAP. Although two kinds of colocalization indices indicated that there was a substantial correlation between MTCL1 or MTCL2 and MTs, the values were relatively low compared with those between MAP4 and MTs (Fig. 2F). These results support the notion that MTCL1 and MTCL2 form a unique family of the MT lattice-binding proteins different from classical MAPs, such as MAP4.

MTCL2 interacts with MTs via the C-terminal conserved region

To determine the molecular basis of the subcellular localization of MTCL2, we subdivided the molecule into three fragments (N, M and C in Fig. 3A) and examined their localization in HeLa-K cells (Fig. 3B). As expected, the C fragment containing the region corresponding to MTCL1 C-MTBD (hereafter referred to as the KR-rich region; Fig. 1A; Fig. S1C) exhibited clear localization on the MT lattice (top and right panels in Fig. 3B). Direct binding of the C-terminal region with MTs was confirmed using a shorter fragment of MTCL2 (CT1) that still contained the KR-rich region (Fig. 3A,C); CT1 fused with maltose-binding protein (MBP), but not MBP alone, co-sedimented with MTs *in vitro* when purified from *Escherichia coli* and mixed with paclitaxel-stabilized MTs. The KR-rich region alone also exhibited localization on MTs (Figs 3D and 4C,D), whereas deletion of the KR-rich region impaired the localization of full-length MTCL2 on MTs (Figs 3A and 4A,B). Taken together with the results that the N and M fragments did not colocalize with MTs (Fig. 3B), these results indicate that MTCL2 has a single MT-binding region at the C-terminus, as predicted from the sequence comparison between MTCL1 and MTCL2 (Fig. S1).

We have previously shown that the C-MTBD of MTCL1 has MT-stabilizing activity (Abdul Kader et al., 2017; Sato et al., 2014). This activity can be monitored by its ability to strongly enhance acetylated tubulin signals and induce MT bundles when expressed in HeLa-K cells (Fig. 4C,E) (Abdul Kader et al., 2017). We noticed that the KR-rich region of MTCL2 did not show these abilities strongly (Fig. 4C,E). These results suggest that the sequence divergence from MTCL1 (Fig. S1C) has weakened the MT-stabilizing activity of the MT-binding region of MTCL2 and made it similar to MTCL1 N-MTBD, which induced MT bundles only when it is oligomerized through the central coiled-coil region (Abdul Kader et al., 2017). To assess this possibility, we first examined whether the coiled-coil region of MTCL2 exhibits homo-interaction activity by using N and M fragments tagged with streptavidin-binding peptide (SBP) or V5 peptide. When the fragments with a different tag were expressed in HEK293T cells in various combinations, homo- but not hetero-interactions were detected for the N and M fragments in pulldown experiments using streptavidin-conjugated resin (Fig. 3E). This finding indicates that the central coiled-coil region of MTCL2 mediated parallel oligomerization of MTCL2, similar to MTCL1. Fig. 3F demonstrates that the C fragment expressed in HeLa-K cells acquired strong MT-bundling activity when fused with the M fragment. These results support the notion that MTCL2 mainly functions as an MT crosslinking protein by directly interacting with MTs via the C-terminus and forming parallel oligomers via the central coiled-coil region.

MTCL2 associates with the Golgi via the N-terminal coiled-coil region

In addition to the MT-associating activity of the C fragment of MTCL2, Fig. 3B revealed a strong association activity of the N fragment with the Golgi membrane. This finding was unexpected because, as for MTCL1, we have failed to identify the region responsible for its Golgi association (our unpublished results). This characteristic activity of the N fragment of MTCL2 contrasted sharply with that of the M fragment, which distributed diffusely without showing any discrete localizations by itself (middle panels in Fig. 3B). These results suggest that MTCL2 is associated with MTs and the Golgi membrane separately through the C- and N-terminal regions, respectively. Considering that the C fragment did not exhibit preferential localization to the perinuclear region (top panels in Fig. 3B), this dual binding activity of MTCL2 might enable the protein to exhibit the preferential association with the perinuclear MTs around the Golgi.

To identify mutations that disrupt the Golgi association of the N fragment, we first performed deletion mapping of a region responsible for this Golgi-association activity and found that the most N-terminal region highly diverged from MTCL1 was dispensable (NΔN in Fig. 5A,B). However, subsequent analysis did not allow us to confine the responsible region narrower than 431 amino acids covering the six N-terminal CC motifs (CC1–CCL6) and an additional ∼40 amino acid sequence downstream of CCL6, which we named the Golgi-localizing essential domain (GLED) (Fig. 5A,B; Fig. S3A,B). We then examined the effects of point mutations in the coiled-coil motifs of the N fragment. At first, four leucine residues appearing in every seven amino acids in the first half of CC1 were mutated to proline (4LP) to disrupt the α-helix itself, or alanine (4LA) to preserve the α-helical structure but suppress its hydrophobic coiled-coil interactions (Fig. 5C). Importantly, not only 4LP mutation but also the 4LA mutation was found to be sufficient to disrupt the Golgi localization of the N fragment (Fig. 5D). These results indicate that the coiled-coil interaction through the first half of CC1 is crucial for the Golgi association of the N fragment. We confirmed that the 4LA mutations

Journal of Cell Science (2022) 135, jcs259374. doi:10.1242/jcs.259374

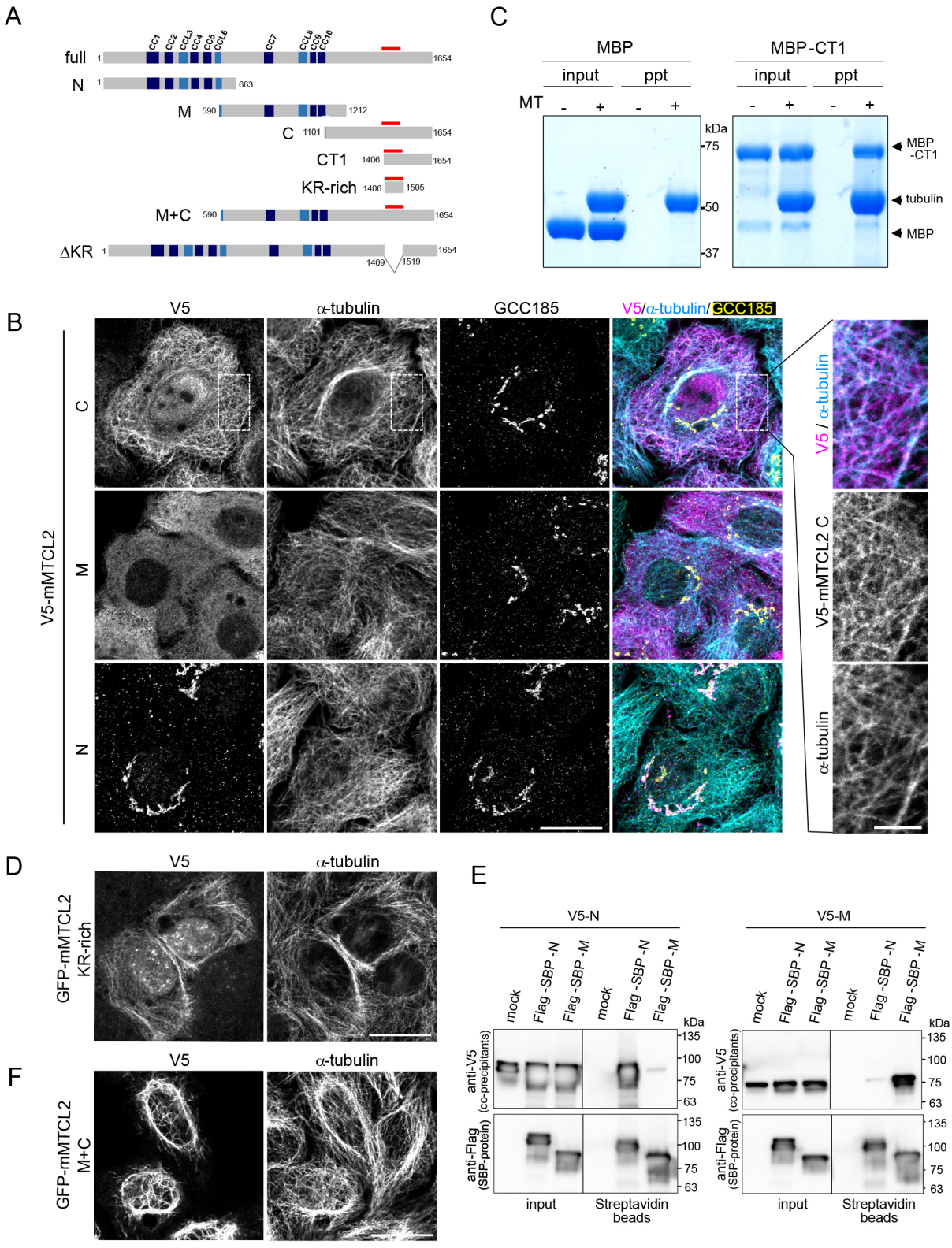

Fig. 3. See next page for legend.

did not disrupt the co-assembling activity of the N fragment (Fig. S3C), likely owing to the homo-interaction of the remaining coiled-coil motifs. This finding indicates that a partial disturbance of the oligomerization state of the N fragment is sufficient to disrupt the Golgi association.

Next, we examined whether these mutations affected the subcellular localization of full-length MTCL2. In these experiments, the expression of exogenous MTCL2 was induced at the endogenous levels in MTCL2-knockdown cells to exclude the effect of endogenous MTCL2 (see Materials and Methods).

Journal of Cell Science (2022) 135, jcs259374. doi:10.1242/jcs.259374

Fig. 3. MTCL2 directly associates with MTs via the C-terminal KR-rich region. (A) MTCL2 deletion mutants related to this figure. Red bars indicate the position of the KR-rich region. (B) Subcellular localization of V5-C (top), -M (middle), and -N (bottom) in HeLa-K cells. The antibodies used are indicated at the top. Scale bar: 20 µm. The boxed region of a V5-C-expressing cell is enlarged in the right panels. Scale bar: 5 µm. Note that the C fragment is colocalized with MTs almost completely, whereas the N fragment is localized to the Golgi distinctly. (C) MBP-fused CT1 purified from *Escherichia coli* was examined for MT pulldown experiments. MBP-CT1 but not MBP was precipitated only when paclitaxel-stabilized MTs were included. ppt represents the MT precipitate obtained after centrifugation (200,000 ***g***) for 20 min at 25°C. (D) Subcellular localization of the GFP-KR-rich region in HeLa-K cells. Scale bar: 20 µm. (E) V5-N (left panels) or V5-M (right panels) were expressed in HEK293T cells together with the indicated proteins and subjected to pulldown assays using streptavidin-conjugated beads. In the mock sample, an empty backbone vector for Flag-SBP constructs was co-transfected. (F) Subcellular localization of V5-M+C in HeLa-K cells. Scale bar: 20 µm. Images shown are representative of at least two experiments.

In contrast to wild-type MTCL2, which showed preferential localization to the perinuclear MTs, the 4LA mutant was diffusely distributed in the cytoplasm without any condensation around the Golgi (Fig. 5E). Importantly, careful examination revealed its colocalization with MTs (Figs 4A,B and 5F), suggesting that MTCL2 can interact with MTs independently of its Golgi association. These findings indicate that the characteristic perinuclear accumulation of endogenous MTCL2 is the result of its Golgi association through the N-terminal coiled-coil region.

MTCL2 promotes the accumulation of MTs around the Golgi complex

We analyzed the effects of MTCL2 knockdown in HeLa-K cells to explore the physiological function of MTCL2 (Fig. 6), by using heterogeneous stable cells expressing various mMTCL2 mutants in a doxycycline-dependent manner. When the cells were transfected with control siRNA in the absence of doxycycline (without exogenous MTCL2 expression), normal accumulation of MTs around the perinuclear region at which endogenous MTCL2 was concentrated was observed (Fig. 6A,C; Fig. S5E). Alternatively, when cells were subjected to MTCL*2* knockdown in the absence of doxycycline (without exogenous MTCL2 expression), MT accumulation around the perinuclear region was severely reduced (Fig. 6A,C; Fig. S5E). The specificity of these knockdown effects was confirmed by a rescue experiment in which doxycycline was added to induce the expression of RNAi-resistant wild-type MTCL2 (mMTCL2 wt) at endogenous levels (Fig. 6A). Under these conditions, many cells showed restored MT accumulation in the perinuclear region, where exogenous MTCL2 was concentrated. We quantitatively estimated the asymmetric distribution of MTs by calculating the skewness of the intensity distribution of tubulin signals within each cell (Fig. 6B; Fig. S4A,B). In the control cells, the pixel intensity of tubulin signals was distributed with a skewness of 1.02 (median), whereas in MTCL2-knockdown cells, this value decreased to 0.73, indicating a more symmetric distribution of MTs. The expression of RNAi-resistant mMTCL2 restored this value to 1.17, statistically supporting its rescue activity.

Interestingly, MTCL2 knockdown also affected the assembly structure of the Golgi stacks (Fig. S5A). In contrast to control cells, which showed a compact crescent-like morphology of the Golgi ribbon on one side of the nucleus, MTCL2-knockdown cells exhibited abnormally expanded Golgi ribbons along the nucleus. The median expansion angle (θ) of the Golgi apparatus was 65.4° for the control cells, whereas it significantly increased to 82.5° in MTCL2-knockdown cells (Figs S4A,C and S5B). The expression of RNAi-resistant MTCL2 reduced the angle to a median value of 61.0°, indicating that MTCL2 is essential for compact accumulation of the Golgi ribbon. Similar effects of MTCL2 knockdown were observed in RPE1 cells (Fig. S4D). These results demonstrate that MTCL2 plays a key role in promoting the perinuclear accumulation of MTs and increasing the compactness of Golgi ribbons.

Considering the MTCL2 localizations and activities shown in Figs 2, 3 and 4, the above results are highly consistent with the hypothesis that MTCL2 crosslinks MTs on the Golgi membrane, thereby mediating accumulation of MTs around the Golgi ribbon. The effects on the compactness of the Golgi ribbon could also be explained as a secondary effect of MT accumulation, which must attract individual Golgi stacks to each other (see an illustration in Fig. S5C). To assess this hypothesis, we performed the same experiments using stable cells but expressing the 4LA mutant in a doxycycline-dependent manner (Fig. 6C,D; Figs S4A–C, S5B,D). Knockdown effects on MT organization and Golgi ribbon compactness were similarly observed in these stable cells (−dox). However, the expression of the 4LA mutant (+dox) did not restore both phenotypes. These findings indicate the importance of Golgi association in MTCL2 functioning. Through similar experiments, we further confirmed that MTCL2 lacking the MT-binding region (MTCL2 ΔKR) also showed loss of rescue activities against both phenotypes (Figs S4A–C, S5E–G).

Altogether, we conclude that MTCL2 promotes MT accumulation around the Golgi ribbon by exerting its MT crosslinking activity on the Golgi membrane.

MTCL2 depletion results in defects in cell migration

The Golgi ribbon structure and its associated MTs are essential for maintaining directed cell migration owing to their essential roles in the polarized transport of vesicles (Bergmann et al., 1983; Yadav et al., 2009; Miller et al., 2009; Sato et al., 2014; Hurtado et al., 2011). Therefore, we next examined whether MTCL2 depletion affected directed cell migration during the wound healing process *in vitro*.

First, HeLa-K cells transfected with control or MTCL2 siRNA were grown to a confluent monolayer and scratched with a micropipette tip to initiate directional migration into the wound. In control cells at the wound edge, reorientation of the Golgi and elongation of a densely aligned MT toward the wound were observed (Fig. 7A). In MTCL2-knockdown cells, reorientation of the Golgi was reduced but not severely affected. Nevertheless, cells lacking MTCL2 exhibited randomly oriented MTs and failed to align them toward the wound (Fig. 7A).

Despite the significant difference in MT organization in cells at the wound edge, we could not estimate the effects of MTCL2 knockdown on directional migration as the HeLa-K cells migrated very slowly. Thus, we used RPE1 cells to estimate wound healing velocity, and found that cells lacking MTCL2 migrated significantly slower than control cells (Fig. 7B; Movies 1 and 2). Comparison of the normalized areas newly covered by migrated cells revealed that the directed migration velocity of MTCL2-knockdown cells was ∼50% of that of control cells (Fig. 7B, right panel). Time-lapse analysis of differential interference contrast images indicated that cells lacking MTCL2 exhibited abnormally elongated shapes and were less efficient in extending lamellipodia (Movie 2). Reorientation of the Golgi position toward the wound was observed in MTCL2-knockdown cells to a similar extent to in control cells (Fig. 7C,D). In addition, and in contrast to HeLa-K cells, MTCL2-knockdown cells showed polarized elongation of MTs toward the wound (Fig. 7C). However, the proximal ends of

Journal of Cell Science (2022) 135, jcs259374. doi:10.1242/jcs.259374

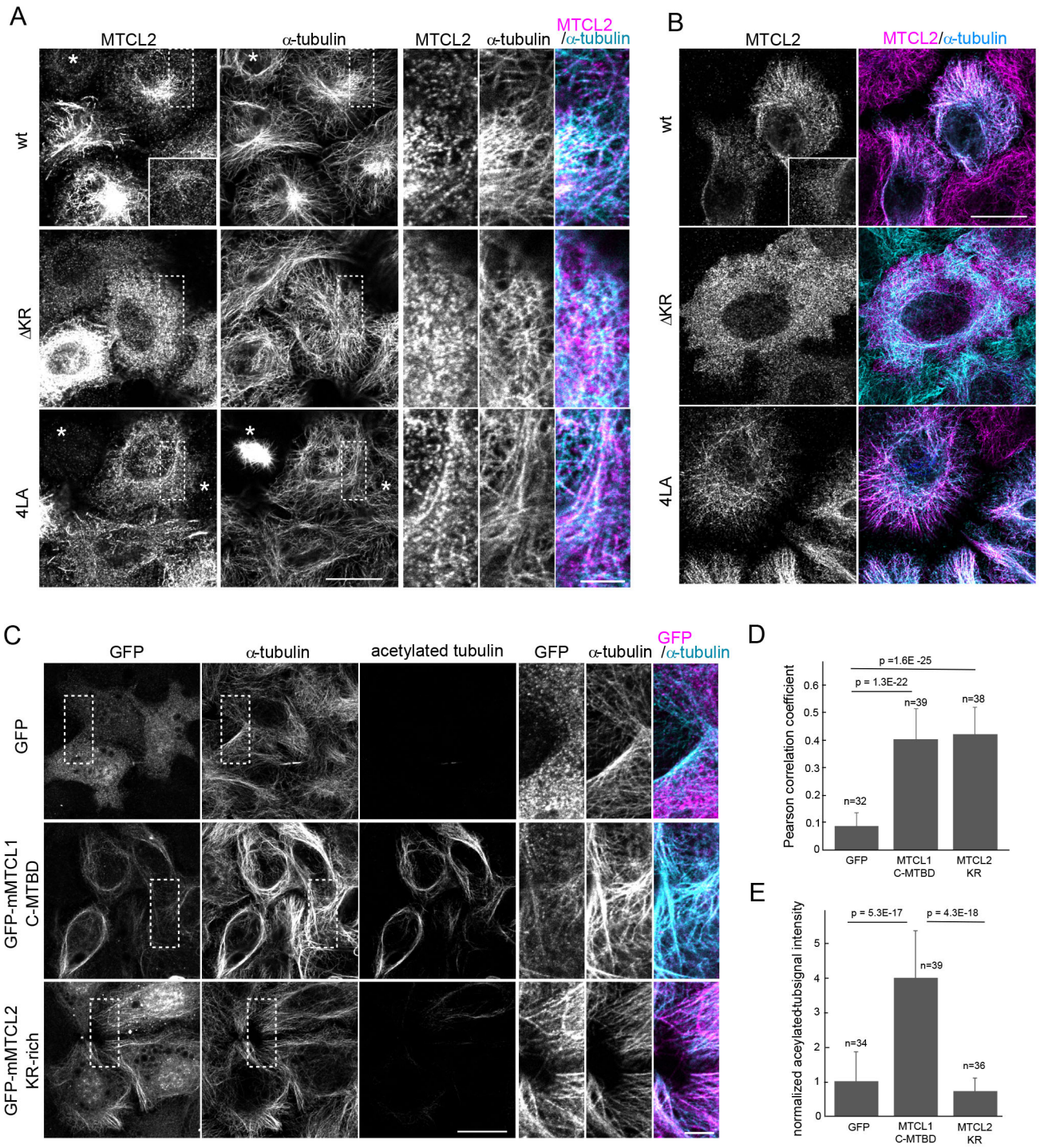

Fig. 4. See next page for legend.

these MTs seemed unfocused. Close inspection revealed that in MTCL2-knockdown cells at the wound edge, the Golgi ribbon was frequently separated from the centrosome and sometimes detached from the nucleus (Fig. 7C,E). As a result, the centrosomal MTs and Golgi-associated MTs elongated from distinct positions and were discerned in many MTCL2-knockdown cells (arrows in Fig. 7C, right panel). By contrast, in control cells, the centrosome and Golgi ribbon were tightly linked near the nucleus, and the proximal ends of the centrosomal and Golgi-associated MTs were indistinguishable. These data suggest an intriguing possibility that MTCL2 might play an essential role in integrating centrosomal and Golgi-associated MTs by crosslinking them on the Golgi membrane.

CLASPs are required for the perinuclear localization of MTCL2

We previously shown that the Golgi association of MTCL1 is mediated by CLASPs and AKAP450 (Sato et al., 2014). Therefore, to identify proteins that mediate the Golgi association of MTCL2, we first examined the effect of knockdown of CLASPs or

Journal of Cell Science (2022) 135, jcs259374. doi:10.1242/jcs.259374

Fig. 4. The KR-rich region is the MT-binding domain of MTCL2 and shows a weak MT-stabilizing activity. (A) Subcellular localizations of exogenously expressed MTCL2 (without tag) detected by anti-SOGA1 (MTCL2) antibody. Expression of mouse MTCL2 wuld-type (wt) or its mutants (ΔKR, 4LA) were induced by adding 100 nM doxycycline in HeLa-K cells stably harboring the corresponding pOSTet15.1 expression vector. Note that the expression of each exogenous protein was induced in MTCL2-knockdown cells to eliminate effects of endogenous MTCL2. An inset in an upper left panel indicates signal intensity of endogenous MTCL2 taken under the same conditions, whereas asterisks indicate cells lacking expression of endogenous as well as exogeneous MTCL2. Scale bar: 20 µm. Boxed regions are areas in which exogenous MTCL2 were expressed at similar levels to the endogenous MTCL2 levels, and are enlarged in the right panels. Scale bar: 5 µm. Note that MTCL2 ΔKR but not 4LA mutant lost MT association activities. Intriguingly, in contrast to the N fragment (see Fig. 3), the ΔKR mutant had no Golgi localization, suggesting that MT binding through the KR-rich region was a prerequisite for the association of full-length MTCL2 with the Golgi membrane. (B) Inability of the ΔKR mutant to associate with MTs was confirmed in cells treated with paclitaxel. (C) HeLa-K cells exogenously expressing GFP, GFP–mMTCL1 C-MTBD or GFP–mMTCL2 KR-rich were stained with the indicated antibodies. Scale bar: 20 µm. Boxed regions are enlarged in right panels. Scale bar: 5 µm. Note that, in contrast to MTCL2 KR, MTCL1 C-MTBD strongly induced tubulin acetylation and MT bundling. Images shown in A–C are representative of at least two experiments. (D) Manders' correlation coefficients (the fraction of GFP signal in pixels containing MT signal) were calculated for immunofluorescence signals of each GFP constructs and MTs. Data represent the means±s.d. for the indicated number (*n*) of regions of interest (ROIs; 100×100 pixels) selected in cytoplasmic regions of cells from two independent experiments. The *P*-value was estimated using an unpaired Student's *t*-test assuming the two-tailed distribution and two-sample unequal variance. (E) Quantitative comparison of acetylated tubulin signals in ROIs in D after normalization by GFP and α-tubulin signal intensities. Data represent the means±s.d. The *P*-value was estimated using an unpaired Student's *t*-test assuming the two-tailed distribution and two-sample unequal variance.

AKAP450 on the subcellular localization of MTCL2. Simultaneous depletion of CLASP1 and CLASP2 profoundly impaired the accumulation of MTCL2 in the perinuclear region and induced an even cytosolic distribution (Fig. 8A; Fig. S6A). An independent set of siRNA oligonucleotides for CLASP1 and CLASP2 also exerted the similar effects (data not shown, see Materials and Methods), indicating that this is the effect results from depletion of the CLASPs. AKAP450 depletion also affected the distribution of MTCL2; however, it did not induce dissociation of MTCL2 from the perinuclear region where the Golgi localizes (Fig. 8A; Fig. S6A). These results are consistent with the report that SOGA1 interacts with CLASP2 (Kruse et al., 2017) and suggest the possibility that CLASPs play major roles in mediating the Golgi association of MTCL2. Consistent with this idea, GFP–CLASP2α (CLASP2α is an isoform of CLASP2) specifically interacted with N but not the M or C fragment of MTCL2 when co-expressed in HEK293T cells and subjected to pulldown experiments (Fig. 8B). The interaction was also observed for the minimum fragment of MTCL2 (CC1-GLED) required for Golgi association (Fig. 8B). However, we unexpectedly observed substantial interactions between GFP–CLASP2α and CC1-GLED with 4LA mutations within CC1. In addition, depletion of CLASPs did not affect the Golgi localization of the N fragment when it was exogenously introduced in HeLa-K cells (Fig. 8C). These results raise the possibility that unknown factors other than CLASPs are involved in the CC1-dependent interaction of MTCL2 with the Golgi membrane. To identify these putative factors, we screened Golgi marker proteins exhibiting the most precise colocalization with the N fragment of MTCL2 (Fig. S7A). Close inspection using super-resolution microscopy revealed that the N fragment showed distinct localization from cis- and trans-Golgi markers; however, it exhibited the most significant colocalization with a cis/medial marker, giantin (also known as GOLGB1) (Linstedt et al., 1995). This finding led us to find that the Golgi localization of the N fragment almost disappeared in cells lacking giantin (Fig. 8C). This observation was also confirmed by an independent siRNA oligonucleotide for giantin (data not shown, see Materials and Methods). Since expression of the N fragment was not reduced in giantin-knockdown cells (Fig. S7B,C), these results indicated that giantin is required for the Golgi association of the MTCL2 N-terminus. Giantin knockdown partially impaired the perinuclear accumulation of endogenous MTCL2 (Fig. 8A; Fig. S6A). Collectively, these findings indicate the possibility that giantin is primarily responsible for the recruitment of MTCL2 to the Golgi membrane in a CC1-dependent manner before CLASP involvement to stabilize the interaction. As endogenous MTCL2 only shows restricted colocalization with CLASPs or giantin (Fig. S7D,E), the interactions between MTCL2 and these proteins might be subsequently weakened to realize its steady-state localization, when it is predominantly associated with the perinuclear MTs.

DISCUSSION

The results of this study demonstrate that the MTCL1 paralog MTCL2 is a novel MT-regulating protein that preferentially associates with perinuclear MTs around the Golgi. Its dual binding activity to MTs and the Golgi, as well as its oligomerizing activity via the coiled-coil region, together with the effects on the MT organization seen upon its knockdown, collectively indicate that MTCL2 functions to crosslink and mediate accumulation of MTs on the Golgi membrane. Our data suggest that this unique activity of MTCL2 plays a significant role in directed migration by integrating the centrosomal and Golgi-nucleated MTs on the Golgi membrane.

MTCL2 depletion severely disrupted the accumulation of MTs around the Golgi and induced random arrays of MTs (Fig. 6A,B; Fig. S5E). Low-dose re-expression of MTCL2 restored the original organization of MTs in a Golgi-binding activity-dependent manner (Fig. 6A,B). These data indicate that MTCL2 plays an indispensable role in the asymmetric organization of global MTs by utilizing the Golgi complex as a foothold for its MT-crosslinking function. These findings also highlight the active role of the Golgi complex in MT organization in interphase cells. Regarding the molecular mechanisms underlying the Golgi association of MTCL2, we provide data indicating the possible involvement of CLASPs and giantin. CLASPs have been shown to play essential roles in development of Golgi-associated MTs through its plus-end-tracking (+Tips) activity (Efimov et al., 2007; Miller et al., 2009). Our results suggest that CLASPs also regulate MTs through its novel activity to facilitate the perinuclear condensation of MTCL2 (Fig. S6B). Here, we demonstrated that CLASP2 interacted with the Golgi association region of MTCL2 (CC1-GLED fragment) independently of the 4LA mutation, and was not necessarily required for recruitment of the CC1-GLED fragment to the Golgi membrane (Fig. 8B,C). These data reveal the presence of complicated mechanisms in the Golgi association of MTCL2, and suggest the presence of multiple and sequential interactions between the MTCL2 N-terminus and several Golgi-resident proteins. This is consistent with the fact that the Golgi association of MTCL2 requires a long amino acid sequence covering 430 amino acids (Fig. 5A). Here, we provide data indicating that one of the candidate molecules for these Golgi-resident proteins is giantin, a large coiled-coil protein, which is known to have a role in ER-Golgi traffic (Alvarez et al., 2001; Sönnichsen et al., 1998). As demonstrated for another golgin

Journal of Cell Science (2022) 135, jcs259374. doi:10.1242/jcs.259374

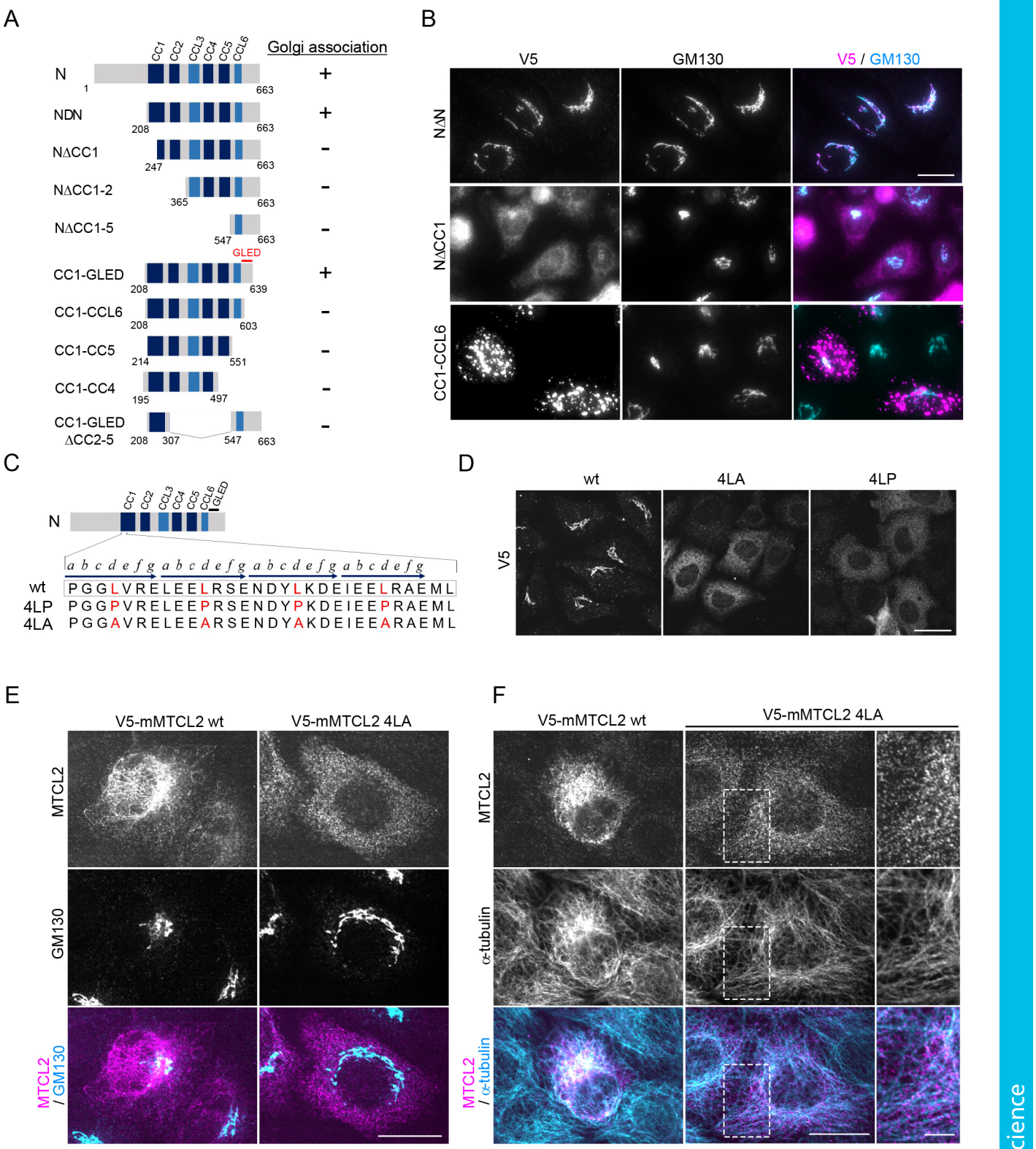

Fig. 5. MTCL2 associates with the Golgi membrane via the N-terminal coiled-coil region. (A) MTCL2 deletion mutants related to this figure and the summary of their Golgi association activity. (B) Subcellular localization of the indicated mutants in HeLa-K cells. Scale bar: 20 µm. (C) Amino acid sequence of the first half of MTCL2 CC1 and positions of four leucine residues mutated in this study (red). The characteristic seven-residue repeats are indicated by horizontal arrows, and the positions of each amino acid in a repeat are indicated by italic letters (*a* to *g*). (D) Subcellular localization of the indicated N fragment mutants in HeLa-K cells was examined using anti-V5 antibody. Scale bar: 20 µm. (E,F) Subcellular localization of V5–mMTCL2 wild-type (wt) or 4LA mutant in HeLa-K cells analyzed using anti-SOGA1 (MTCL2) antibody together with anti-GM130 (E) or anti-α-tubulin (F). Scale bars: 20 µm. Boxed regions in F are enlarged in the right panels. Scale bar: 5 µm. Note that the expression of each exogenous protein was induced in MTCL2-knockdown cells and suppressed to the endogenous level. Images shown are representative of at least two experiments.

Journal of Cell Science (2022) 135, jcs259374. doi:10.1242/jcs.259374

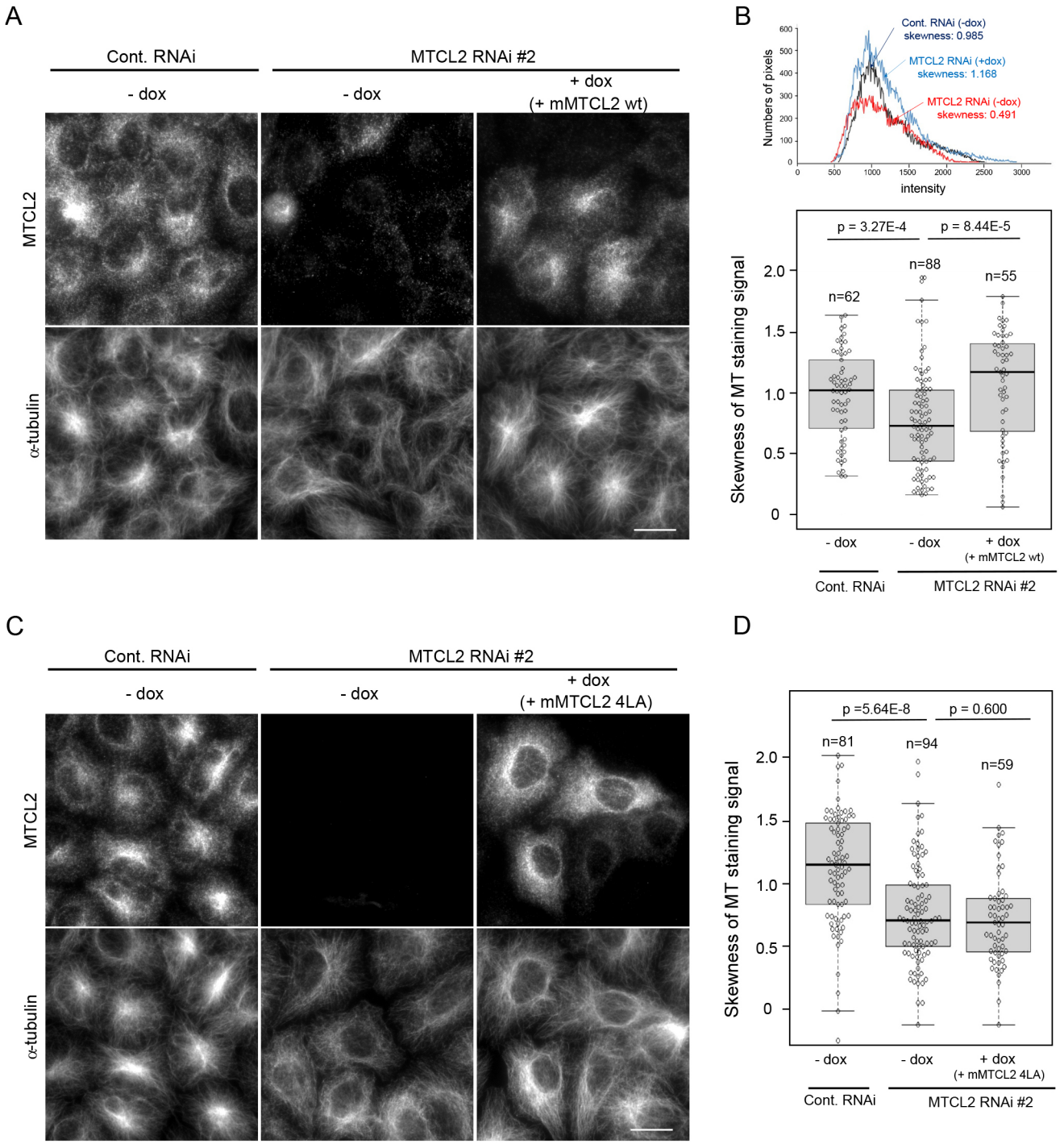

Fig. 6. MTCL2 promotes the perinuclear accumulation of MTs in a Golgi-association-dependent manner. (A) HeLa-K cells stably harboring pOSTet15.1 expression vector for mouse MTCL2 (without tag) were transfected with siRNAs for control or MTCL2 knockdown (#2) in the presence or absence of 100 nM doxycycline (dox) and doubly stained with anti-SOGA1 (MTCL2) and anti-α-tubulin antibody, as indicated on the left. Scale bar: 20 µm. (B) Extent of MT accumulation was quantitatively estimated by calculating the skewness of the pixel intensity distribution for tubulin signals in each cell. The top panel shows typical data on the tubulin signal distributions and their skewness values, indicating that the asymmetries of tubulin signal distribution are compromised in MTCL2-knockdown cells. The bottom is a box plot of the skewness distribution in each condition. Data represent the results of the indicated number (*n*) of cells from a typical experiment (biological replicates; see Materials and Methods). The *P*-values were estimated using the Wilcoxon test. Statistical data of technical replicates (three independent experiments) are demonstrated in Fig. S4. (C) HeLa-K cells stably harboring pOSTet15.1 expression vector for mouse MTCL2 4LA were subjected to the same experimental procedure as in (A). Scale bar: 20 µm. (D) MT accumulation data in C was quantitatively analyzed as in B. For the box plots in B,D, the box represents the 25–75th percentiles, and the median is indicated. The whiskers are drawn based on 1.5× the interquartile range value.

protein, GCC185 (also known as GCC2), our present data might indicate an additional role of giantin to regulate MT organization (Fig. S6B) (Efimov et al., 2007; Wong and Munro, 2014).

The complexity of the Golgi-binding mechanisms of MTCL2 is also indicated by comparison with MTCL1, which also exhibits a subcellular localization strikingly similar to that of MTCL2

Journal of Cell Science (2022) 135, jcs259374. doi:10.1242/jcs.259374

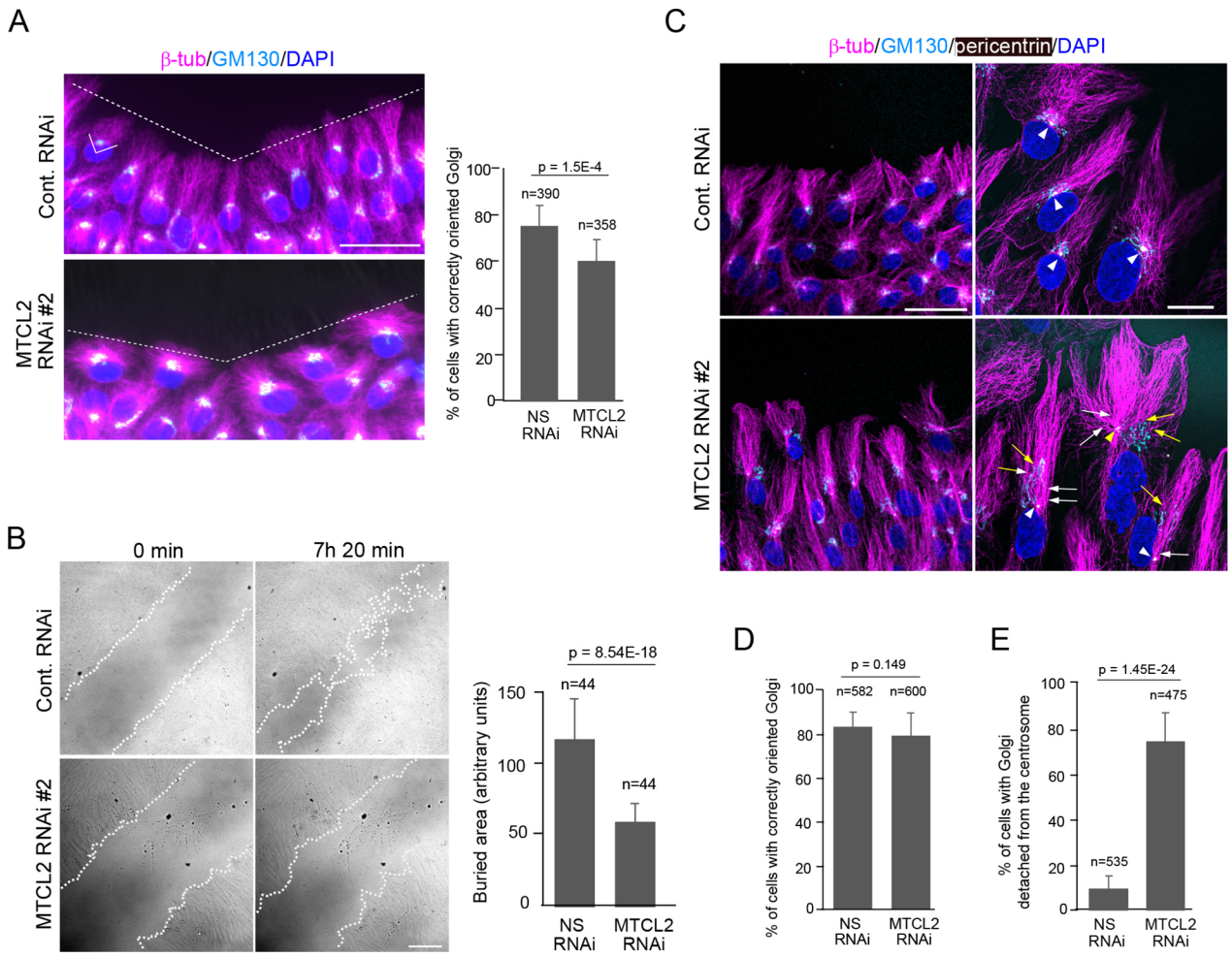

Fig. 7. MTCL2 depletion results in defective cell migration. (A) Confluent monolayers of HeLa-K cells subjected to control or MTCL2 RNAi were fixed and stained with the indicated antibodies 6 h after wounding. Cells facing the wound edges (white dotted lines) are shown. Scale bar: 50 µm. Note that MTCL2-depleted cells did not polarize MT arrays toward the wound. The right panel indicates the percentage of wound-edge cells with correctly oriented Golgi, defined as those falling in the indicated quadrant (white line) concerning the wound edge. Data represent the means±s.d. for the indicated number (*n*) of cells from two independent experiments. The *P*-value was estimated using an unpaired Student's *t*-test assuming the two-tailed distribution and two-sample unequal variance. (B) Differential interference contrast images of wound healing RPE1 cells at 0 min and 7 h 20 min after wounding. White dotted line delineates the wound edges. Scale bar: 200 µm. Right panel indicates quantified data on the areas newly buried by cells after wounding. Data represent the mean±s.d. of 44 fields taken from two independent experiments. The *P*-value was estimated using an unpaired Student's *t*-test assuming the two-tailed distribution and two-sample unequal variance. (C) RPE1 cells subjected to wound healing analysis in B were fixed and stained with the indicated antibodies. Cells facing the wound edges are shown. Right panels show an enlarged view. Arrowheads indicate the positions of the centrosomes. Note that MTCL2-depleted cells exhibit separation of the centrosome and Golgi. The centrosomes frequently show significant detachment from the perinuclear region (see yellow arrowhead). White and yellow arrows indicate MTs emanating from the centrosome and the Golgi, respectively. Scale bars: 50 µm and 20 µm (enlarged right panels). (D) Golgi orientation was quantified for wound healing RPE1 cells, as indicated in A. Data represent the means±s.d. for the indicated number (*n*) of cells from two independent experiments. The *P*-value was estimated using an unpaired Student's *t*-test assuming the two-tailed distribution and two-sample unequal variance. (E) Percentage of wound-edge cells with Golgi detached from the centrosome. Data represent the means±s.d. for the indicated number (*n*) of cells from two independent experiments. The *P*-value was estimated using an unpaired Student's *t*-test assuming the two-tailed distribution and two-sample unequal variance.

(Fig. 2E) (Sato et al., 2014). As for MTCL1, we have failed to identify the Golgi association region, despite the significant amino acid similarity of its N-terminal coiled-coil motifs with MTCL2 (Fig. S1B). Instead, the seamless exchange of the highly conserved CC1 sequence between MTCL1 and MTCL2 was sufficient to disrupt the Golgi localization of the MTCL2 N fragment (Fig. S3D). This indicates that the Golgi-binding mechanisms of MTCL proteins are not based on simple coiled-coil interactions but consist of sophisticated protein–protein interactions that are highly differentiated between these paralogs. This is consistent with the fact that the Golgi association of MTCL2 strongly depends on CLASPs but not AKAP450 (Fig. 8A), whereas the Golgi association of MTCL1 depends on both proteins almost evenly (Sato et al., 2014).

It is also noteworthy that full-length MTCL2 lacking MT-binding activity (MTCL2 ΔKR) was distributed diffusely without Golgi localization (Fig. 4A; Fig. S5E,F). Since the N-terminal fragment associates with the Golgi membrane clearly (Fig. 3B), this indicates that MT binding through the C-terminal region could be a prerequisite for Golgi association via the N-terminal coiled-coil region, and implies intramolecular regulation of the Golgi binding of MTCL2. The fact that endogenous MTCL2 does not exhibit complete colocalization with the Golgi complex (Fig. 2A) further suggests the presence of additional mechanisms that regulate the

Journal of Cell Science (2022) 135, jcs259374. doi:10.1242/jcs.259374

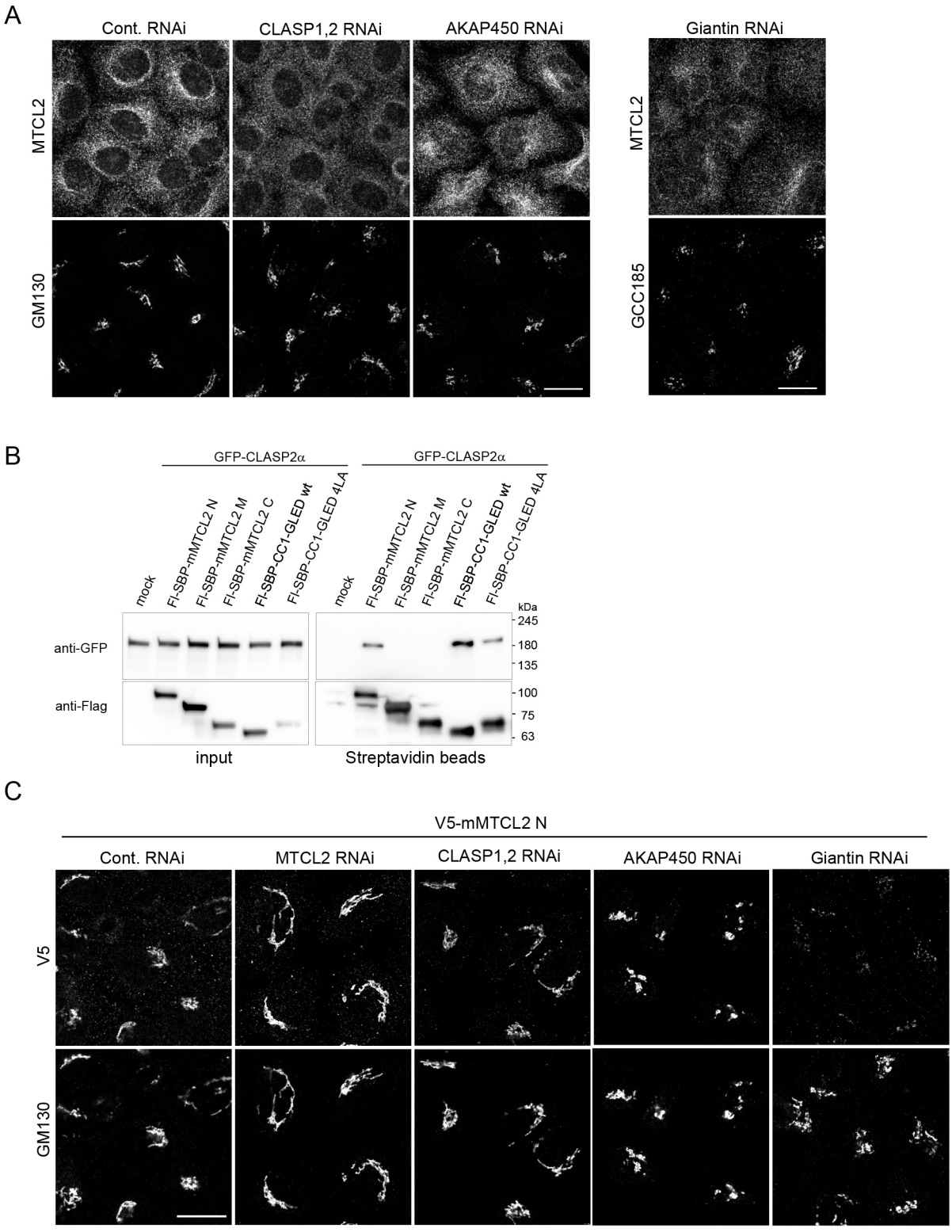

Fig. 8. CLASPs and giantin are involved in the Golgi association of MTCL2. (A) HeLa-K cells subjected to the indicated knockdown were stained by anti-SOGA1 (MTCL2) together with anti-GM130 or anti-GCC185 antibodies as indicated. Scale bars: 20 µm. (B) GFP–CLASP2α was expressed in HEK293T cells together with the indicated Flag–SBP-tagged proteins and subjected to pulldown assays using streptavidin-conjugated beads. (C) V5-N was expressed in HeLa-K cells subjected to the indicated knockdown and examined for the Golgi association. Scale bar: 20 µm. Images shown are representative of at least two experiments.

balance between the dual binding activities of MTCL2 to MTs and the Golgi membrane.

Our results indicate that MTCL2 is expressed in several cultured cells simultaneously with MTCL1 (Fig. 1C) (Sato et al., 2014). The tissue distribution patterns of MTCL2 are also similar to those of MTCL1 (Fig. 1D) (Satake et al., 2017). These results raise questions regarding how cells utilize these MTCL proteins differentially. A clue can be drawn from the previously reported result that, in contrast

Journal of Cell Science (2022) 135, jcs259374. doi:10.1242/jcs.259374

to MTCL2, MTCL1 knockdown does not change the global organization of MTs significantly, but only reduces a specific subpopulation of MTs specifically stained with an anti-acetylated tubulin antibody (Sato et al., 2014). This MT subpopulation corresponds to stable MTs that are nucleated from the Golgi membrane with the aid of CLASPs and AKAP450 (Chabin-Brion et al., 2001; Efimov et al., 2007; Rivero et al., 2009). Considering that MTCL1 stabilizes and crosslinks this specific MT subpopulation via its C-MTBD and N-MTBD, respectively (Abdul Kader et al., 2017; Sato et al., 2014), these results suggest that the target of MTCL1 action is restricted to the Golgi-associated MTs. By contrast, as we demonstrated here, MTCL2 knockdown dramatically changes the global organization of MTs (Fig. 6A), and the MT-binding region of MTCL2 lacks strong activity to stabilize MTs (Fig. 4C,E). These results suggest the possibility that, in contrast to MTCL1, the target of MTCL2 action might not be restricted to the Golgi-nucleated MTs. In extreme cases, MTCL2 might crosslink any kinds of MTs running nearby the Golgi complex. This idea is consistent with the present observation that MTCL2 is required to integrate centrosomal and Golgi-derived MTs on the Golgi membrane. Distinct involvement of AKAP450 in Golgi recruitment might be one of the bases of these functional differences between MTCL1 and MTCL2. Further assessment of the Golgi-recruiting mechanisms of each protein will better elucidate this issue.

In this study, we established the presence of a new family of MT-regulating proteins, the MTCL family, the members of which exhibit intermittent interactions with the MT lattice (Fig. 2E). Although the molecular basis of this interaction is not known yet, an intriguing possibility is that they specifically recognize tubulins within GTP islands, which have been shown to distribute along MTs stochastically (Dimitrov et al., 2008). No matter how the mechanism is, the functions of MTCL proteins are expected to be tightly linked with vertebrate-specific cellular structures and functions because their clear orthologs are only found in vertebrates. We propose that this gene product should be called MTCL2 instead of SOGA1 because our results demonstrate that its full-length form is a functional homolog of MTCL1 and its cleaved form is not observed ubiquitously. This claim is also based on the fact that we failed to confirm the presence of a putative internal signal sequence as well as Atg16- and Rab5-binding motifs in the MTCL2 sequence, all of which have been discussed previously (Fig. 1A) (Cowerd et al., 2010).

MATERIALS AND METHODS

Vector production

The cDNA clone encoding full-length mMTCL2 (GenBank accession number AK147227) was purchased from Danaform (Kanagawa, Japan). After confirming sequence identity with NM_001164663, a DNA fragment corresponding to the MTCL2 open reading frame was subcloned into the expression vector pCAGGS-V5 (Yamashita et al., 2010). Subsequently, several deletion mutants of MTCL2 were constructed in pCAGGS-V5, pEGFP-c2 (Takara Bio Inc., Japan), or pMal-c5x (New England Biolabs). To establish heterogeneous stable transformants, mMTCL2 and its mutants with or without a 6×V5-tag were subcloned in pOSTet15.1 (kindly provided by Yoshihiro Miwa, University of Tsukuba, Japan), an Epstein–Barr virus-based extrachromosomal vector carrying a replication origin and replication initiation factor sufficient for autonomous replication in human cells (Tanaka et al., 1999). Mouse MTCL1 cDNA (GenBank accession number AK147691) was used as described previously (Sato et al., 2013). Expression vector for GFP-CLASP2α was a gift from Ikuko Hayashi (Yokohama City University, Japan).

Antibodies

To detect MTCL1 and MTCL2, anti-KIAA0802 (sc-84865) from Santa Cruz Biotechnology and anti-SOGA1 (HPA043992) from Sigma-Aldrich were used, respectively. To detect other proteins, the following antibodies were used: anti-α-tubulin (sc-32293), anti-acetylated tubulin (sc-23950), anti-MAP4 (sc-67152), anti-GFP (sc-9996) and anti-CLASP2 (sc-376496) from Santa Cruz Biotechnology; anti-V5 (R960-25) from Thermo Fisher Scientific; anti-GM130 (610822) and anti-GS28 (611184) from BD Transduction Laboratories; anti-GAPDH (5G4) from HyTest Ltd.; anti-giantin (ab37266) and anti-pericentrin (ab4448) from Abcam; anti-GCC185 from Bethyl Laboratories; anti-Flag (F3165) from Sigma-Aldrich; anti-β-tubulin (MAB3408) from Merck Millipore; anti-CLASP1 (MAB9736) from Abnova; anti-AKAP450 from Novus Biologicals; anti-Golgin97 (also known as GOLGA1) (D8P2K) from Cell Signaling Technology.

Cell culture and plasmid transfection

HeLa-K (HeLa-Kyoto) cells were a generous gift from Dr S. Tsukita (Osaka University, Osaka, Japan). HEK293T and the hTERT-immortalized human retinal pigment epithelial (RPE1) cells were purchased from ATCC (American Type Culture Collection). HepG2 cells were purchased from JCRB (Japan Collection of Research Bioresources) cell bank. HeLa-K, HEK293T and HepG2 cells were cultured in Dulbecco's modified Eagle's medium (DMEM, low glucose; Nissui, Japan) containing 10% fetal bovine serum, 100 U/ml penicillin, 100 µg/ml streptomycin and 1 mM glutamine at 37°C in 5% CO_2. RPE1 cells were maintained in a 1:1 mixture of DMEM/Ham's F12 (FUJIFILM Wako Pure Chemical Corporation, Japan) containing 10% fetal bovine serum, 100 U/ml penicillin, 100 µg/ml streptomycin, 10 µg/ml hygromycin B, and 1 mM glutamine at 37°C in 5% CO_2. Paclitaxel treatment (0.2 µM) was performed for 2 h.

For immunofluorescence analysis, cells were seeded on coverslips in 24-well plates and coated with atelocollagen (0.5 mg/ml; IPC-50, KOKEN, Japan). Plasmid transfections were performed using polyethyleneimine (Polysciences, Inc.) for HEK293T cells or Lipofectamine LTX (Life Technologies Corporation) for HeLa-K cells according to the manufacturer's instructions. To establish heterogenous stable HeLa-K cells expressing mMTCL2 or its mutants in a doxycycline-dependent manner, cells were transfected with the pOSTet15.1 expression vector encoding the appropriate MTCL2 cDNA. The following day, cells were reseeded at 1/20th of the cell density and subjected to selection using a medium containing 800 µg/ml G418 disulfate (Nacalai Tesque, Japan) for more than 6 days. Surviving cells were used in subsequent experiments without cloning.

RNAi experiments and wound healing assays

siRNAs for human MTCL2 and giantin were designed to target the following sequences: MTCL#2, 5′-GAGCGACCGAGAGAGCATTCC-3′; #5, 5′-CTGAAGTACCGCTCGCTCT-3′; and giantin, 5′-GAGAAGA-CCTCTCATATTT-3′. The target sites for CLASP1, CLASP2, and AKAP450 have been described previously: CLASP1, 5′-GGATGATT-TACAAGACTGG-3′; CLASP2, 5′-GACATACATGGGTCTTAGA-3′ (Mimori-Kiyosue et al., 2005); AKAP450, 5′-AACTTTGAAGTTAAC-TATCAA-3′ (Rivero et al., 2009). Another siRNA for CLASPs and giantin targeting the following sequences were also used in experiments whose data are not shown here: CLASP1, 5′-GTGATATTGTGTCCCGCGA-3′; CLASP2, 5′-GTAATTGGTGATGAACTAA-3′; and giantin, 5′-CAGC-TAAAGAGTGTATGGA-3′. A non-silencing RNAi oligonucleotide (All-stars negative control siRNA) was purchased from Qiagen. Cells were seeded on coverslips at densities of 1.2×10^4–4×10^4 cells and transfected with siRNAs at final concentrations of 10–17 nM using RNAiMax (Life Technologies Corporation) according to the manufacturer's instructions. siRNA transfection was repeated the day after medium change, and cells were subjected to immunofluorescence analysis on day 3. For rescue experiments, heterogeneous stable HeLa-K cells expressing mMTCL2 were subjected to a similar protocol, except that 100 ng/ml of doxycycline was always included in the medium after the first siRNA transfection. For wound healing analysis, HeLa-K cell monolayers subjected to RNAi were scratched with a micropipette tip on day 4. RPE1 cells were seeded at 5×10^4 cells in one compartment of a 35 mm glass bottom culture dish separated into four compartments (Greiner, 627870) after coating with 10 µg/ml fibronectin (FUJIFILM, Japan, 063-05591). The siRNA transfections

were performed as described above. Wounds were created on day 4 by scratching the cell monolayers with a micropipette tip and subjected to live imaging.

Cell extraction and western blotting

Cell extracts were prepared by adding RIPA buffer (25 mM Tris-HCl pH 7.5, 150 mM NaCl, 1% NP40, 1% deoxycholic acid and 0.1% SDS) containing a protease inhibitor cocktail (Sigma-Aldrich, P8340) followed by brief sonication and centrifugation (15,000 ***g***, 15 min). For tissue distribution analysis of MTCL2, mouse tissue lysates prepared in a previous study were used (Satake et al., 2017). Samples were separated by SDS-PAGE and transferred to PVDF membranes. Blots were incubated in blocking buffer containing 5% (w/v) dried skim milk in 8.1 mM $Na_2HPO_4.12H_2O$, 1.47 mM KH_2PO_4, 137 mM NaCl, 2.7 mM KCl and 0.05% Tween 20 (PBST), followed by overnight incubation with the appropriate antibodies diluted in blocking buffer. Dilutions of anti-SOGA1 and anti-GAPDH antibodies were 1:1000 and 1:5000, respectively. The secondary antibodies were diluted at 1:2000. Blots were then exposed to horseradish peroxidase (HRP)-conjugated secondary antibodies (GE Healthcare) diluted in blocking buffer for 60 min at room temperature (RT) and washed again. Blots were visualized using Immobilon Western Chemiluminescent HRP Substrate (Millipore) or ECL western blotting detection system (GE Healthcare). Chemiluminescence was quantified using the ImageQuant LAS4000 Luminescent Image Analyzer (GE Healthcare). The full, uncropped blots of all western blot data are provided in Fig. S8.

Immunofluorescence staining

In most cases, except the experiments in Fig. S2, cells were fixed with cold methanol for 10 min at −20°C, followed by blocking with 10% (v/v) fetal bovine serum in PBST. To visualize the subcellular localization of exogenous MTCL2, cells were treated with modified PBST containing 0.5% Triton X-100 instead of Tween 20 for 10 min after methanol fixation. To examine different fixation conditions, cells were fixed with 4% paraformaldehyde in BRB80 buffer (80 mM PIPES-KOH pH 6.8, 1 mM $MgCl_2$ and 1 mM EGTA), with or without pre-extraction using BRB80 buffer supplemented with 4 mM EGTA and 0.5% Triton X-100, for 30 s at 37°C. After fixation and blocking, samples were incubated with appropriate primary antibodies diluted in 10 mM Tris-HCl pH 7.5, 150 mM NaCl, 0.01% (v/v) Tween 20 (TBST) containing 0.1% (w/v) bovine serum albumin (BSA) for 45 min at RT, except for MTCL1, MTCL2 and MAP4 staining, which was performed overnight at 4°C. After washing with PBST, samples were visualized with the appropriate secondary antibodies conjugated with Alexa Fluor 488, 555 or 647 (Life Technologies Corporation) by incubating for 45 min at RT. Antibodies were diluted as follows: anti-KIAA0802 (1:1000), anti-SOGA1 (1:2000), anti-α-tubulin (1:1000), anti-β-tubulin (1:2000), anti-acetylated tubulin (1:1000), anti-V5 (1:4000), anti-GM130 (1:1000), anti-GS28 (1:300), anti-GFP (1:2000), anti-MAP4 (1:1000), anti-pericentrin (1:1000), anti-CLASP1 (1:500), anti-CLASP2 (1:500), anti-giantin (1:1000), anti-GCC185 (1:2000; anti-AKAP450 (1:500); anti-Golgin97 (1:1000). All secondary antibodies were used at a 1:2000 dilution. The nuclei were counterstained with DAPI (MBL, Japan) at a 1:2000 dilution in PBST during the final wash. For image acquisition, samples on coverslips were mounted onto glass slides in Prolong Diamond Antifade Mountant (Thermo Fisher Scientific).

Image acquisition and processing

High-resolution images were acquired using a Leica SP8 laser scanning confocal microscopy system equipped with an HC PL APO 63×/1.40 NA Oil 2 objective, using the Hybrid Detector in photon-counting mode. To obtain super-resolution images, HyVolution2 imaging was performed on the same system using the Huygens Essential software (Scientific Volume Imaging) (Borlinghaus and Kappel, 2016). Single confocal slice images are shown in all figures. To obtain wide-view images for quantification in Fig. 6 and Fig. S5, conventional fluorescence images were obtained using an AxioImager ZI microscope (Carl Zeiss, Oberkochen, Germany) equipped with a Plan APCHROMAT 40×/0.95 objective using an Orca II CCD camera (Hamamatsu Photonics, Shizuoka, Japan).

Colocalizations with MTs were assessed by using the Coloc2 plugin implemented in ImageJ software (Fiji). The Pearson correlation coefficient was calculated without using threshold, whereas Manders' correlation coefficient (the fraction of MAP signal in pixels containing MT signal) was calculated based on the threshold determined by a Costes randomization test (50 times; Costes et al., 2004). For statistical analysis of MTCL2 knockdown phenotypes, photographs of several fields containing ∼40 cells with similar densities were taken. All cells in each field were subjected to analysis to avoid selection bias. In rescue experiments, ∼100 cells expressing exogenous MTCL2 at similar expression levels as the endogenous cells were collected from ∼10 fields with similar cell densities. The laterally expanding angle of the Golgi around the nuclei and the skewness of pixel intensity distribution in each cell were quantified using the 'Measure' function of ImageJ software. For live-cell imaging, differential interference contrast images were acquired using a Leica SP8 confocal microscopy system equipped with an HCX PL APO 10×/0.40 NA objective using a 488 nm laser line. Areas newly covered by migrated cells during wound healing for 440 min were estimated using the 'Measure' function of ImageJ software and normalized to the length of the corresponding wound edge at time 0.

MT-binding assay

MBP or MBP–mMTCL1 CT1 was purified from the soluble fraction of *E. coli* according to standard protocols and dialyzed against BRB80 buffer. Each MBP was incubated with paclitaxel-stabilized MTs [final concentrations of both the sample protein and the α-tubulin–β-tubulin (α/β-tubulin) heterodimer were 0.5 mg/ml] in BRB80 supplemented with 1.5 mM $MgCl_2$ and 1 mM GTP for 15 min at RT and subjected to centrifugation (70,000 rpm using a Beckman TLA100.3 rotor) for 20 min at 25°C on a cushion of 40% glycerol in BRB buffer. Following careful removal of the supernatant and glycerol cushion, the resultant MT pellet was gently washed with PBST three times and solubilized with SDS sample buffer (10% β-mercaptoethanol, 125 mM Tris-HCl [pH 6.8], 2% SDS, 10% glycerol and 0.005% Bromophenol Blue) for subsequent SDS-PAGE analysis. The original gel photograph is provided in Fig. S8.

Pulldown experiments

HEK293T cells (∼8×10^6 cells) transfected with appropriate expression vectors were solubilized in 500 µl lysis buffer (20 mM Tris-HCl pH 7.5, 150 mM NaCl, 0.3% Triton X-100, 2 mM $MgCl_2$, 1 mM EGTA) containing a cocktail of protease and phosphatase inhibitors (Roche Applied Science) for 30 min at 4°C. They were then briefly sonicated and centrifuged at 15,000 ***g*** for 30 min. The resulting supernatants were mixed with streptavidin-conjugated magnetic beads (Cytiva) for ∼2 h at 4°C. The beads were collected using a magnet, washed with lysis buffer three times, and then boiled in SDS sample buffer. Proteins released from the beads were subjected to western blotting analysis using the following antibodies: anti-V5 (1:3000), anti-GFP (1:1000), and anti-Flag (1:3000).

Acknowledgements

The authors thank Yoshihiro Miwa (University of Tsukuba) and Ikuko Hayashi (Yokohama City University) for providing the pOSTet15.1 expression vector and GFP–CLASP2α expression vector, respectively.

Competing interests

The authors declare no competing or financial interests.

Author contributions

Conceptualization: A.S.; Investigation: R.M., M.M., S.M., Y.I., A.S.; Resources: C.Y.; Writing - original draft: A.S.; Writing - review & editing: A.S.; Supervision: A.S.

Funding

This work was supported by KAKENHI (to A.S.) (grant numbers 16H04765 and 19H03228) of the Ministry of Education, Culture, Sports, Science, and Technology (MEXT) of Japan.

Peer review history

The peer review history is available online at https://journals.biologists.com/jcs/article-lookup/doi/10.1242/jcs.259374.

References

Abdul Kader, M., Satake, T., Yoshida, M., Hayashi, I. and Suzuki, A. (2017). Molecular basis of the microtubule-regulating activity of microtubule crosslinking factor 1. *PLoS ONE* **12**, e0182641. doi:10.1371/journal.pone.0182641

Alvarez, C., Garcia-Mata, R., Hauri, H.-P. and Sztul, E. (2001). The p115-interactive proteins GM130 and giantin participate in endoplasmic reticulum-golgi traffic. *J. Biol. Chem.* **276**, 2693-2700. doi:10.1074/jbc.M007957200

Bartolini, F. and Gundersen, G. G. (2006). Generation of noncentrosomal microtubule arrays. *J. Cell Sci.* **119**, 4155-4163. doi:10.1242/jcs.03227

Bergmann, J. E., Kupfer, A. and Singer, S. J. (1983). Membrane insertion at the leading edge of motile fibroblasts. *Proc. Natl. Acad. Sci. USA* **80**, 1367-1371. doi:10.1073/pnas.80.5.1367

Borlinghaus, R. T. and Kappel, C. (2016). HyVolution—the smart path to confocal super-resolution. *Nat. Methods* **13**, i-iii. doi:10.1038/nmeth.f.392

Chabin-Brion, K., Marceiller, J., Perez, F., Settegrana, C., Drechou, A., Durand, G. and Poüs, C. (2001). The Golgi complex is a microtubule-organizing organelle. *Mol. Biol. Cell* **12**, 2047-2060. doi:10.1091/mbc.12.7.2047

Chapin, S. J. and Bulinski, J. C. (1991). Non-neuronal 210×10(3) Mr microtubule-associated protein (MAP4) contains a domain homologous to the microtubule-binding domains of neuronal MAP2 and tau. *J. Cell Sci.* **98**, 27-36. doi:10.1242/jcs.98.1.27

Combs, T. P. and Marliss, E. B. (2014). Adiponectin signaling in the liver. *Rev. Endocr. Metab. Disord.* **15**, 137-147. doi:10.1007/s11154-013-9280-6

Conduit, P. T., Wainman, A. and Raff, J. W. (2015). Centrosome function and assembly in animal cells. *Nat. Rev. Mol. Cell Biol.* **16**, 611-624. doi:10.1038/nrm4062

Costes, S. V., Daelemans, D., Cho, E. H., Dobbin, Z., Pavlakis, G. and Lockett, S. (2004). Automatic and quantitative measurement of protein-protein colocalization in live cells. *Biophys. J.* **86**, 3993-4003. doi:10.1529/biophysj.103.038422

Cowerd, R. B., Asmar, M. M., Alderman, J. M., Alderman, E. A., Garland, A. L., Busby, W. H., Bodnar, W. M., Rusyn, I., Medoff, B. D., Tisch, R. et al. (2010). Adiponectin lowers glucose production by increasing SOGA. *Am. J. Pathol.* **177**, 1936-1945. doi:10.2353/ajpath.2010.100363

Dimitrov, A., Quesnoit, M., Moutel, S., Cantaloube, I., Poüs, C. and Perez, F. (2008). Detection of GTP-tubulin conformation in vivo reveals a role for GTP remnants in microtubule rescues. *Science* **322**, 1353-1356. doi:10.1126/science.1165401

Efimov, A., Kharitonov, A., Efimova, N., Loncarek, J., Miller, P. M., Andreyeva, N., Gleeson, P., Galjart, N., Maia, A. R. R., McLeod, I. X. et al. (2007). Asymmetric CLASP-dependent nucleation of noncentrosomal microtubules at the trans-Golgi network. *Dev. Cell* **12**, 917-930. doi:10.1016/j.devcel.2007.04.002

Hurtado, L., Caballero, C., Gavilan, M. P., Cardenas, J., Bornens, M. and Rios, R. M. (2011). Disconnecting the Golgi ribbon from the centrosome prevents directional cell migration and ciliogenesis. *J. Cell Biol.* **193**, 917-933. doi:10.1083/jcb.201011014

Kruse, R., Krantz, J., Barker, N., Coletta, R. L., Rafikov, R., Luo, M., Højlund, K., Mandarino, L. J. and Langlais, P. R. (2017). Characterization of the CLASP2 protein interaction network identifies SOGA1 as a microtubule-associated protein. *Mol. Cell. Proteomics* **16**, 1718-1735. doi:10.1074/mcp.RA117.000011

Linstedt, A. D., Foguet, M., Renz, M., Seelig, H. P., Glick, B. S. and Hauri, H. P. (1995). A C-terminally-anchored Golgi protein is inserted into the endoplasmic reticulum and then transported to the Golgi apparatus. *Proc. Natl. Acad. Sci. USA* **92**, 5102-5105. doi:10.1073/pnas.92.11.5102

Lupas, A., Van Dyke, M. and Stock, J. (1991). Predicting coiled coils from protein sequences. *Science* **252**, 1162-1164. doi:10.1126/science.252.5009.1162

Meiring, J. C. M., Shneyer, B. I. and Akhmanova, A. (2020). Generation and regulation of microtubule network asymmetry to drive cell polarity. *Curr. Opin. Cell Biol.* **62**, 86-95. doi:10.1016/j.ceb.2019.10.004

Miller, P. M., Folkmann, A. W., Maia, A. R. R., Efimova, N., Efimov, A. and Kaverina, I. (2009). Golgi-derived CLASP-dependent microtubules control Golgi organization and polarized trafficking in motile cells. *Nat. Cell Biol.* **11**, 1069-1080. doi:10.1038/ncb1920

Mimori-Kiyosue, Y., Grigoriev, I., Lansbergen, G., Sasaki, H., Matsui, C., Severin, F., Galjart, N., Grosveld, F., Vorobjev, I., Tsukita, S. et al. (2005). CLASP1 and CLASP2 bind to EB1 and regulate microtubule plus-end dynamics at the cell cortex. *J. Cell Biol.* **168**, 141-153. doi:10.1083/jcb.200405094

Nishita, M., Satake, T., Minami, Y. and Suzuki, A. (2017). Regulatory mechanisms and cellular functions of non-centrosomal microtubules. *J. Biochem.* **109**, 20029-20034. doi:10.1093/jb/mvx018

Rivero, S., Cardenas, J., Bornens, M. and Rios, R. M. (2009). Microtubule nucleation at the cis-side of the Golgi apparatus requires AKAP450 and GM130. *EMBO J.* **28**, 1016-1028. doi:10.1038/emboj.2009.47

Sanders, A. A. W. M. and Kaverina, I. (2015). Nucleation and dynamics of Golgi-derived microtubules. *Front. Neurosci.* **9**, 1-7. doi:10.3389/fnins.2015.00431

Satake, T., Yamashita, K., Hayashi, K., Miyatake, S., Tamura-Nakano, M., Doi, H., Furuta, Y., Shioi, G., Miura, E., Takeo, Y. H. et al. (2017). MTCL1 plays an essential role in maintaining Purkinje neuron axon initial segment. *EMBO J.* **36**, 1227-1242. doi:10.15252/embj.201695630

Sato, Y., Akitsu, M., Amano, Y., Yamashita, K., Ide, M., Shimada, K., Yamashita, A., Hirano, H., Arakawa, N., Maki, T. et al. (2013). The novel PAR-1-binding protein MTCL1 has crucial roles in organizing microtubules in polarizing epithelial cells. *J. Cell Sci.* **126**, 4671-4683. doi:10.1242/jcs.127845

Sato, Y., Hayashi, K., Amano, Y., Takahashi, M., Yonemura, S., Hayashi, I., Hirose, H., Ohno, S. and Suzuki, A. (2014). MTCL1 crosslinks and stabilizes non-centrosomal microtubules on the Golgi membrane. *Nat. Commun.* **5**, 5266. doi:10.1038/ncomms6266

Sönnichsen, B., Lowe, M., Levine, T., Jämsä, E., Dirac-Svejstrup, B. and Warren, G. (1998). A role for giantin in docking COPI vesicles to Golgi membranes. *J. Cell Biol.* **140**, 1013-1021. doi:10.1083/jcb.140.5.1013

Tanaka, J., Miwa, Y., Miyoshi, K., Ueno, A. and Inoue, H. (1999). Construction of Epstein-Barr virus-based expression vector containing mini-oriP. *Biochem. Biophys. Res. Commun.* **264**, 938-943. doi:10.1006/bbrc.1999.1617

Vorobjev, I. A. and Nadezhdina, E. S. (1987). The centrosome and its role in the organization of microtubules. *Int. Rev. Cytol.* **106**, 227-293. doi:10.1016/S0074-7696(08)61714-3

Wei, J.-H. and Seemann, J. (2010). Unraveling the Golgi ribbon. *Traffic* **11**, 1391-1400. doi:10.1111/j.1600-0854.2010.01114.x

Wong, M. and Munro, S. (2014). The specificity of vesicle traffic to the Golgi is encoded in the golgin coiled-coil proteins. *Science* **346**, 1256898. doi:10.1126/science.1256898

Wu, J. and Akhmanova, A. (2017). Microtubule-organizing centers. *Annu. Rev. Cell Dev. Biol.* **33**, 51-75. doi:10.1146/annurev-cellbio-100616-060615

Wu, J., de Heus, C., Liu, Q., Bouchet, B. P., Noordstra, I., Jiang, K., Hua, S., Martin, M., Yang, C., Grigoriev, I. et al. (2016). Molecular pathway of microtubule organization at the Golgi apparatus. *Dev. Cell* **39**, 44-60. doi:10.1016/j.devcel.2016.08.009

Yadav, S., Puri, S. and Linstedt, A. D. (2009). A primary role for Golgi positioning in directed secretion, cell polarity, and wound healing. *Mol. Biol. Cell* **20**, 1728-1736. doi:10.1091/mbc.e08-10-1077

Yamashita, K., Suzuki, A., Satoh, Y., Ide, M., Amano, Y., Masuda-Hirata, M., Hayashi, Y. K., Hamada, K., Ogata, K. and Ohno, S. (2010). The 8th and 9th tandem spectrin-like repeats of utrophin cooperatively form a functional unit to interact with polarity-regulating kinase PAR-1b. *Biochem. Biophys. Res. Commun.* **391**, 812-817. doi:10.1016/j.bbrc.2009.11.144

Yang, C., Wu, J., de Heus, C., Grigoriev, I., Liv, N., Yao, Y., Smal, I., Meijering, E., Klumperman, J., Qi, R. Z. et al. (2017). EB1 and EB3 regulate microtubule minus end organization and Golgi morphology. *J. Cell Biol.* **216**, 3179-3198. doi:10.1083/jcb.201701024

Supplementary Figure S1

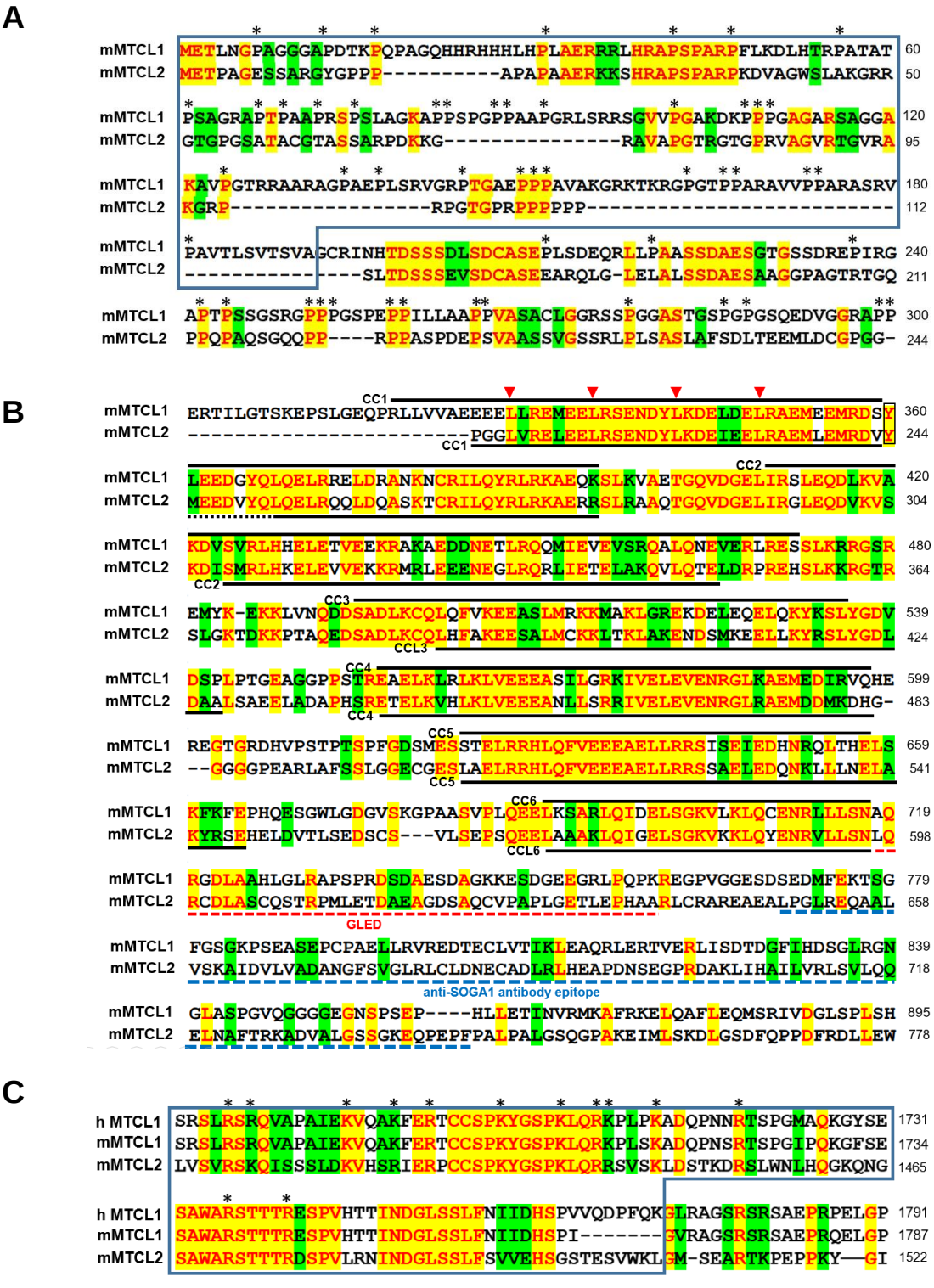

Fig. S1. Sequence alignment of amino acid sequences of mouse MTCL1 and 2.

(A) The N-terminal sequences. Boxed region corresponds to N-MTBD of MTCL1. Asterisks indicate the positions of proline highly condensed in this region. (B) The N-terminal coiled-coil region. The positions of each coiled-coil motif (CC) or coiled-coil-like motif (CCL) of MTCL1 or 2 are indicated by bold lines on the top or bottom of each sequence, respectively. GLED sequence of MTCL2 is underlined by a red dashed line. Four leucine residues mutated in 4LA or 4LP mutants are indicated red arrowheads. A tyrosine residue that disrupts the periodicity of CC1 is boxed. Blue dotted lines indicate the region corresponding to the epitope for anti-SOGA1 antibody. (C) The sequences of the C-terminal MT-binding regions. Because MTCL1 C-MTBD (boxed) was defined for human protein (Sato et al., 2013), the human sequence of MTCL1 is also included in this alignment. The region of mouse MTCL2 corresponding to MTCL1 C-MTBD is designated the “KR-rich region” since the conserved basic residues (asterisks) are condensed.

Supplementary Figure S2

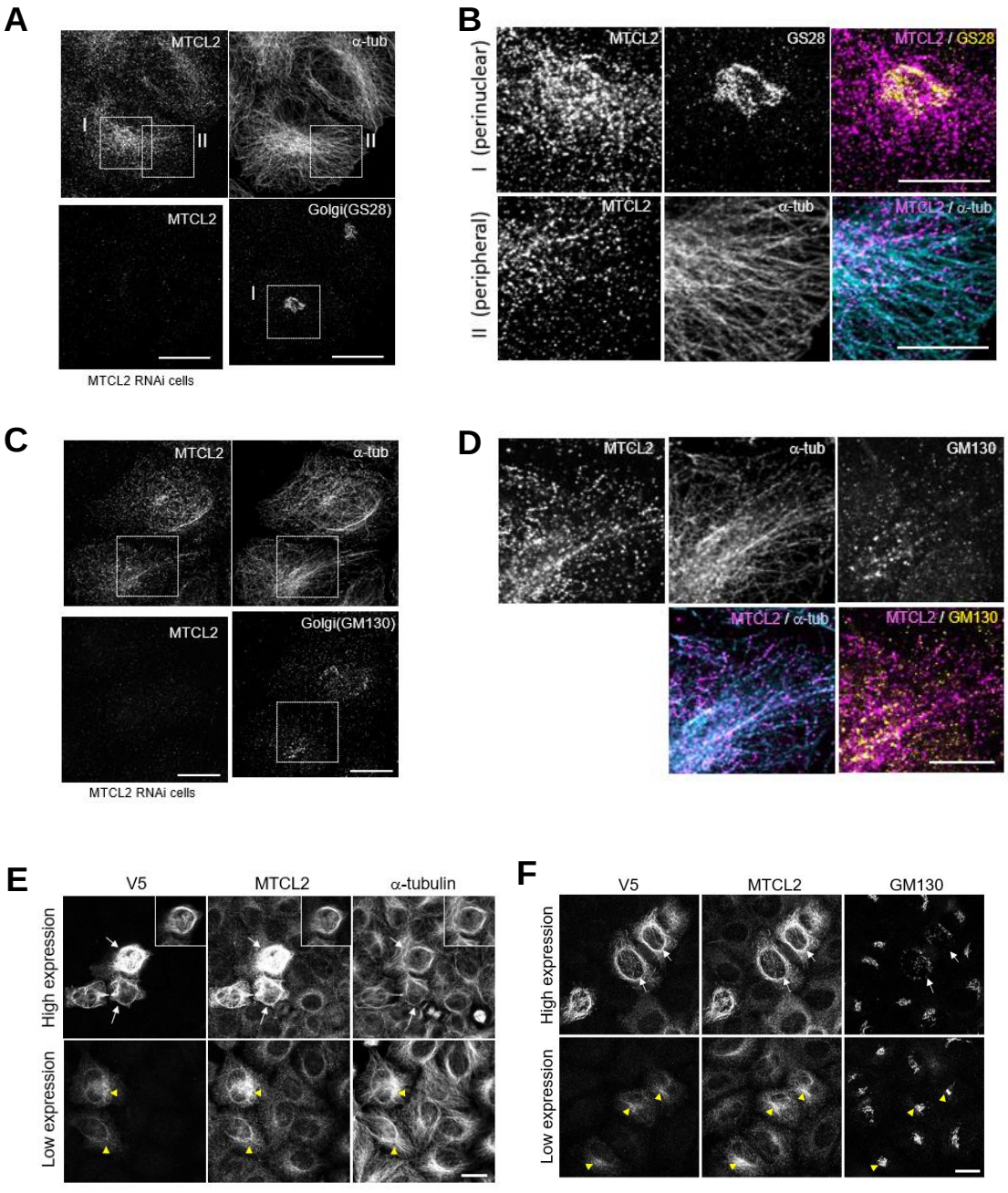

Fig. S2. Confirmations of subcellular localization of MTCL2.

(A) HeLa-K cells fixed with 4% paraformaldehyde were stained with anti-SOGA1 (MTCL2) together with anti-α-tubulin and anti-GS28 antibody. The specificity of anti-SOGA1 signals is indicated by their disappearance in MTCL*2*-knockdown cells subjected to the same procedures (see a lower left panel). Scale bar: 20 μm. (B) Boxed regions in (A) are enlarged to examine the colocalization of MTCL2 on the Golgi and MTs more closely. Scale bar: 10 μm. (C) HeLa-K cells were fixed with 4% paraformaldehyde after brief treatment of an extraction buffer containing 0.5% TX-100 and 4 mM EGTA. The specificity of anti-SOGA1 staining signals is indicated by their disappearance in MTCL*2*-knockdown cells subjected to the same procedures (see a lower left panel). Scale bar: 20 μm. (D). The boxed region in (C) is enlarged to examine the colocalization of MTCL2 on the Golgi and MTs more closely. Scale bar: 10 μm. (E and F) Localization of exogenously expressed MTCL2 mimics that of endogenous proteins at low expression levels. HeLa-K cells stably harboring 6xV5-tagged mouse MTCL2 expression vector (pOSTet15.1) were cultured in the presence of 100 ng/mL doxycycline and stained with the indicated antibodies. Scale bar: 20 μm. Arrows indicate cells highly expressing exogenous MTCL2, whereas yellow arrowheads indicate cells expressing exogenous MTCL2 at a level comparable to endogenous MTCL2. The insets in (E) show alternative images of a cell located at the center of the panel, in which contrasts of the individual staining signals are adjusted separately to provide unsaturated images.

Supplementary Figure S3

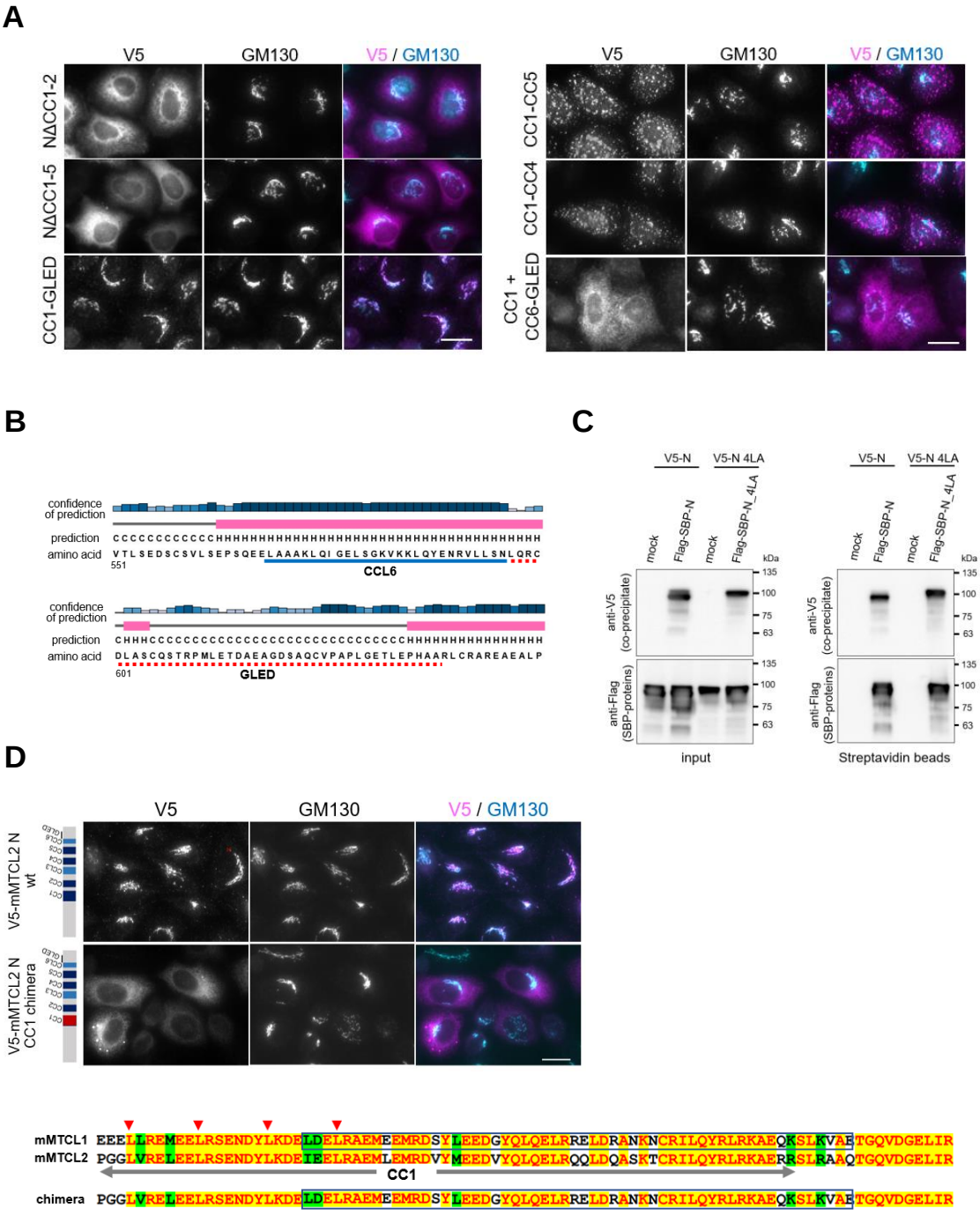

Fig. S3. The essential sequence required for the Golgi association of the MTCL2 N fragment.

(A) Subcellular localization of the indicated mutants expressed in HeLa-K cells (see Fig. 5A). Scale bar: 20 μm. (B) The amino acid sequence of GLED and its secondary structure redicted using PSIPED (http://bioinf.cs.ucl.ac.uk/psipred/). (C) A streptavidin pull-down experiment was performed for soluble extracts (input) of HEK293 cells expressing V5-N with Flag-SBP-N or V5-N 4LA with Flag-SBP-N 4LA, as indicated. In mock samples, empty backbone vectors for Flag-SBP constructs were transfected with each V5 construct. (D) Subcellular localization of the CC1 chimera of the N fragment, in which the highly conserved CC1 sequence of MTCL2 was seamlessly exchanged with that of MTCL1. Scale bar, 20 μm. The amino acid sequence of CC1 in the chimera mutant is shown below.

Supplementary Figure S4

A

wt

MT distribution (skewness)

	n			p-value	
	NS	KD	res	NS/KD	KD/rescue
1st	56	56	23	1.50E-04	2.03E-03
2nd	99	79	58	3.96E-07	8.40E-03
3rd	62	88	55	3.27E-04	8.44E-05
sum	217	223	136	5.77E-10	1.71E-06

4LA

	n			p-value	
	NS	KD	res	NS/KD	KD/rescue
1st	81	94	51	5.64E-08	0.600
2nd	123	93	71	1.86E-03	0.270
3rd	77	125	93	0.050	0.890
sum	281	312	215	7.46E-11	0.984

ΔKR

	n			p-value	
	NS	KD	res	NS/KD	KD/rescue
1st	65	56	45	2.01E-02	0.490
2nd	112	106	58	5.88E-05	0.534
3rd	73	106	47	7.37E-03	0.072
sum	250	268	150	1.07E-07	0.1056

Golgi ribbon expansion angle

	n			p-value	
	NS	KD	res	NS/KD	KD/rescue
1st	196	149	196	2.77E-13	2.20E-16#
2nd	358	339	177	2.20E-16#	2.20E-16#
3rd	114	114	73	1.01E-05	6.85E-05
sum	668	602	446	2.20E-16#	2.20E-16#

	n			p-value	
	NS	KD	res	NS/KD	KD/rescue
1st	85	65	47	6.85E-12	0.579
2nd	134	79	68	4.00E-11	0.766
3rd	120	126	50	8.88E-05	0.028*
sum	339	270	165	2.20E-16	0.265

	n			p-value	
	NS	KD	res	NS/KD	KD/rescue
1st	95	81	56	1.60E-09	0.698
2nd	83	113	88	4.31E-03	1.95E-03*
3rd	102	110	41	6.25E-04	0.169
sum	280	304	185	1.32E-12	3.64E-03*

B

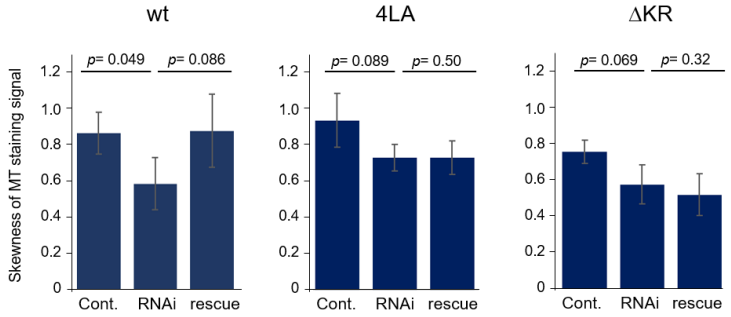

C

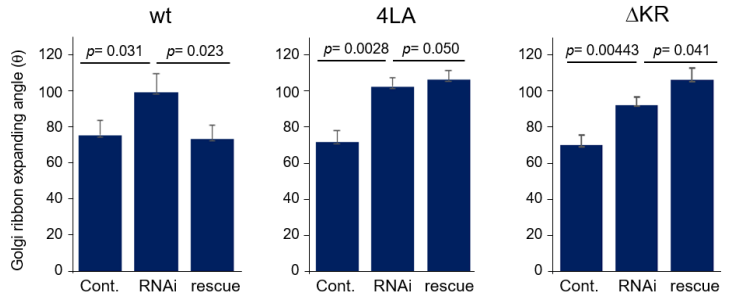

D

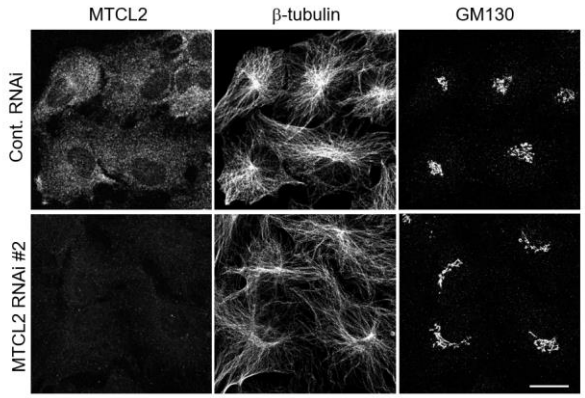

Fig. S4. Statistical data for technical replicates of the rescue experiments.

(A) Numbers of biological replicates (n) and *p* values estimated by the Wilcoxon test are listed for each rescue experiment replicated three times. Top, experiments to examine rescue activity for MT distribution. Bottom, Golgi ribbon compactness. The *p* values indicated by # mean less than 2.20e-16. Expression of MTCL2 mutants (4LA, ΔKR) tended to worsen the knockdown phenotypes of MTCL2, sometimes resulting in low *p* values in KD/rescue comparison, as indicated by asterisks. Note that essential trends of each MTCL2 mutant shown in Fig. 6 and Supplementary Figure S5 are highly reproduced except in an experiment (yellow cell) in which the MTCL2-knockdown effect was rather low. (B and C) Mean of biological replicates in each experiment listed in (A) was averaged in three technical replicates and compared between each condition. Data represent the mean ± S.D. of three independent experiments for MT distribution (B) and Golgi ribbon compactness (C). The *p* value was estimated using Student's t-test assuming a one-tailed distribution and two-sample unequal variance. (D) RPE1 cells transfected with control or MTCL2 siRNAs were subjected to immunofluorescence analysis using the indicated antibodies. Note that reduced accumulation of MTs around the Golgi and lateral expansion of the Golgi ribbon were observed in this cell line. Scale bar: 20 μm.

Supplementary Figure S5

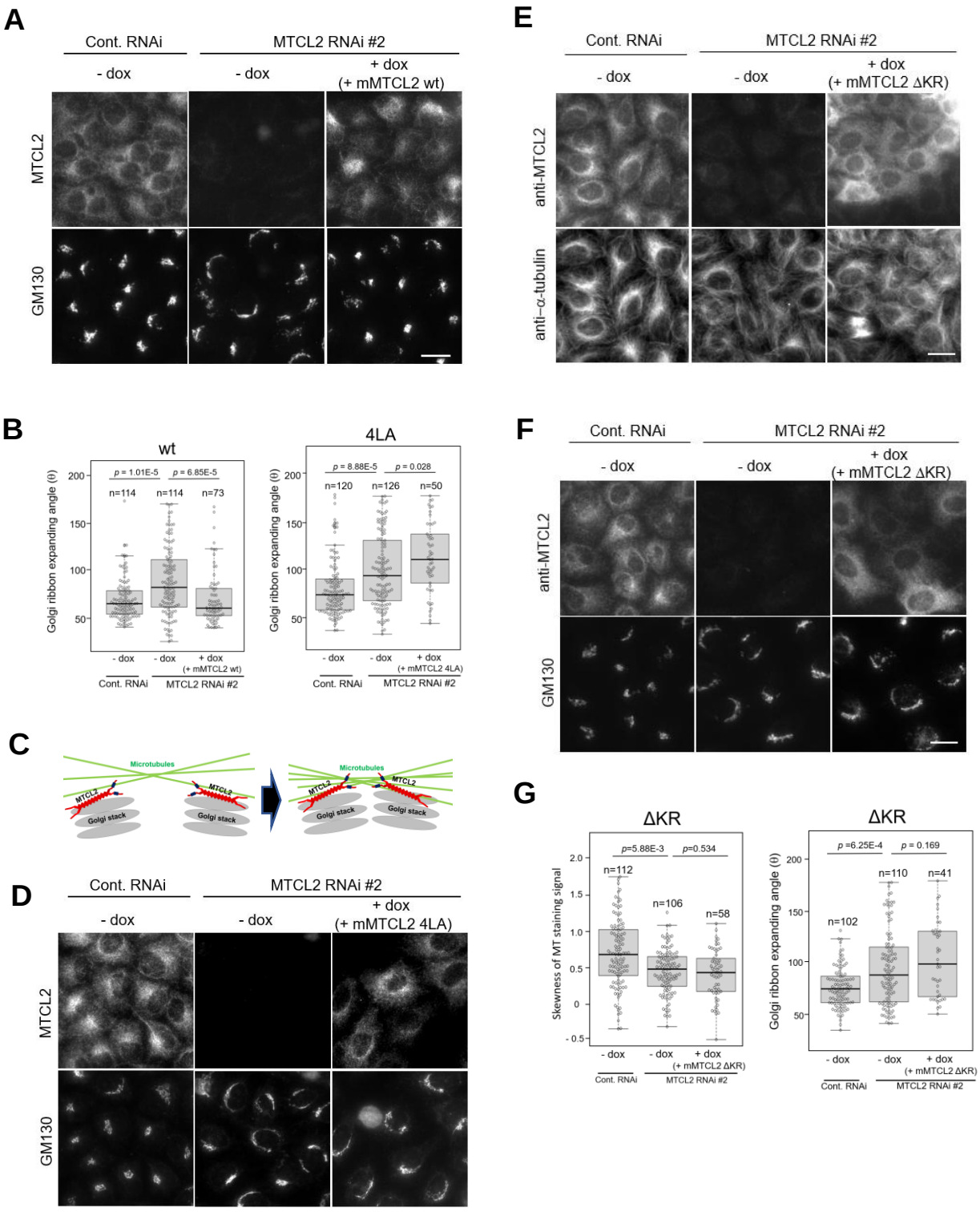

Fig. S5. MTCL2 promotes clustering of the Golgi stacks in a Golgi-association-dependent manner.

(A) HeLa-K cells stably harboring pOSTet15.1 expression vector for mouse MTCL2 were transfected with siRNAs for control or MTCL2 knockdown (#2) in the presence or absence of 100 nM doxycycline and doubly stained with anti-SOGA1 (MTCL2) and anti-GM130 antibodies, as indicated on the left. Note that cells subjected to control RNAi show compact Golgi ribbon structures at one side of the perinuclear region. Such Golgi ribbon structures become laterally expanded around the nucleus in MTCL2-knockdown cells (-dox), whereas exogenous expression of RNAi-resistant MTCL2 (+dox) strongly restores their compactness. Scale bar: 20 μm. (B) Box plots of the angle distribution in each condition (left, data for wt rescue; right, data for 4LA mutant rescue shown in (D)). The lines within each box represent medians. Data represent the results of the indicated number (n) of cells from a typical experiment (biological replicates). The *p* values were estimated using the Wilcoxon test. Statistical data of technical replicates (three independent experiments) are demonstrated in Supplementary Fig. S4.
(C) A model explaining how MT accumulation secondarily increases clustering of individual Golgi stacks.
(D) HeLa-K cells stably harboring pOSTet15.1 expression vector for mouse MTCL2 4LA were subjected to the same experimental procedure as in (A). Note that compactness of Golgi ribbon was not restored by expression of mouse MTCL2 4LA. Scale bar: 20 μm. (E-G) HeLa-K cells stably harboring pOSTet15.1 expression vector for mouse MTCL2 ΔKR were transfected with siRNAs for control or MTCL2 knockdown (#2) in the presence or absence of 100 nM doxycycline (dox). Perinuclear accumulation of MTs (E and left panel in G) and expansion of the Golgi ribbon around the nucleus (F and right panel in G) were analyzed in the same manner as described in (A) and (B). Scale bar: 20 μm.

Supplementary Figure S6

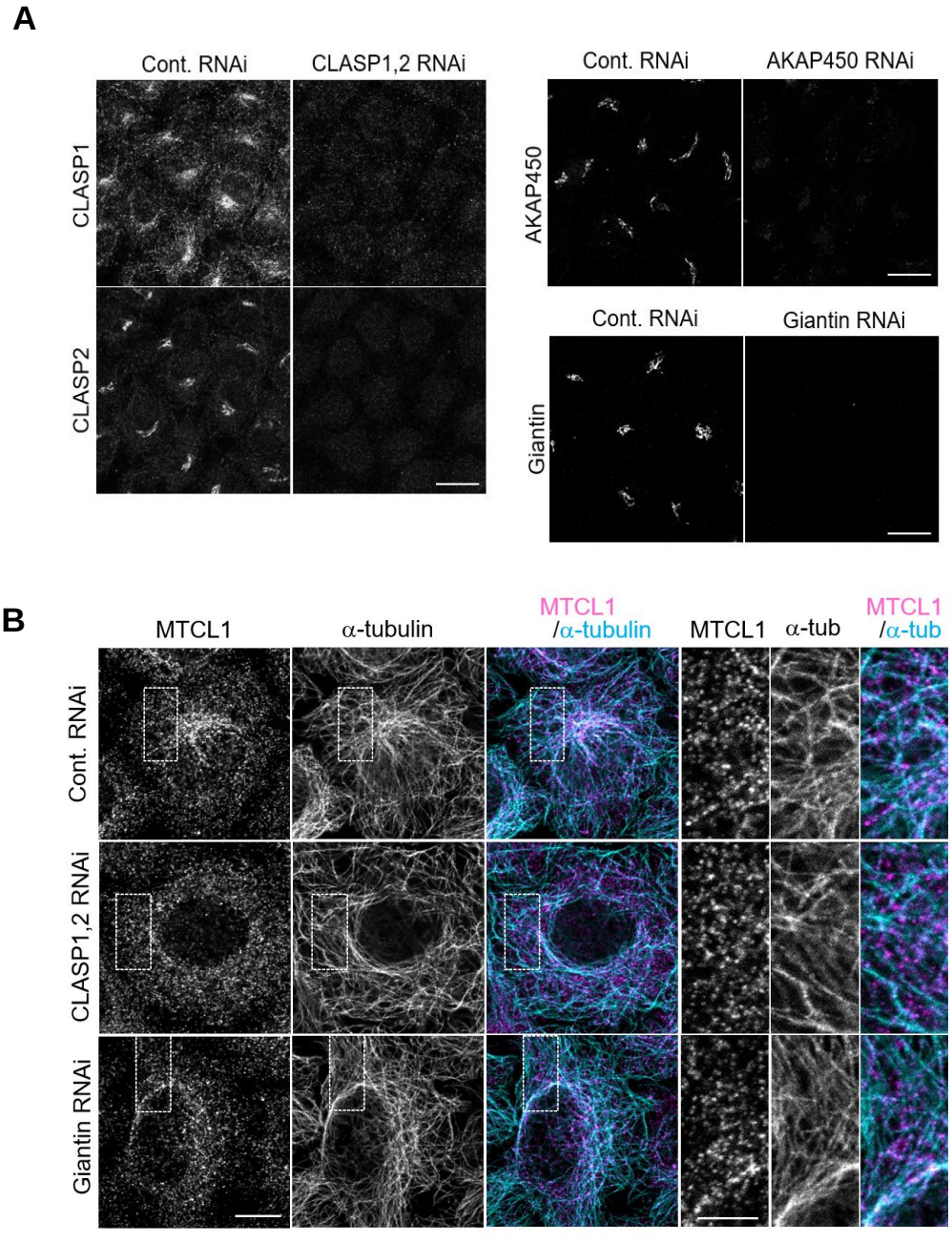

Fig. S6. Knockdown effects of CLASP, AKAP450, and giantin.

(A) Reduced expression of target proteins of the indicated siRNAs is shown. Scale bar: 20 μm. (B) Colocalization of endogenous MTCL2 with MTs in the indicated knockdown cells was examined in HeLa-K cells. Scale bar: 10 μm. Boxed regions are enlarged in the right panels. Scale bar: 5 μm.

Supplementary Figure S7

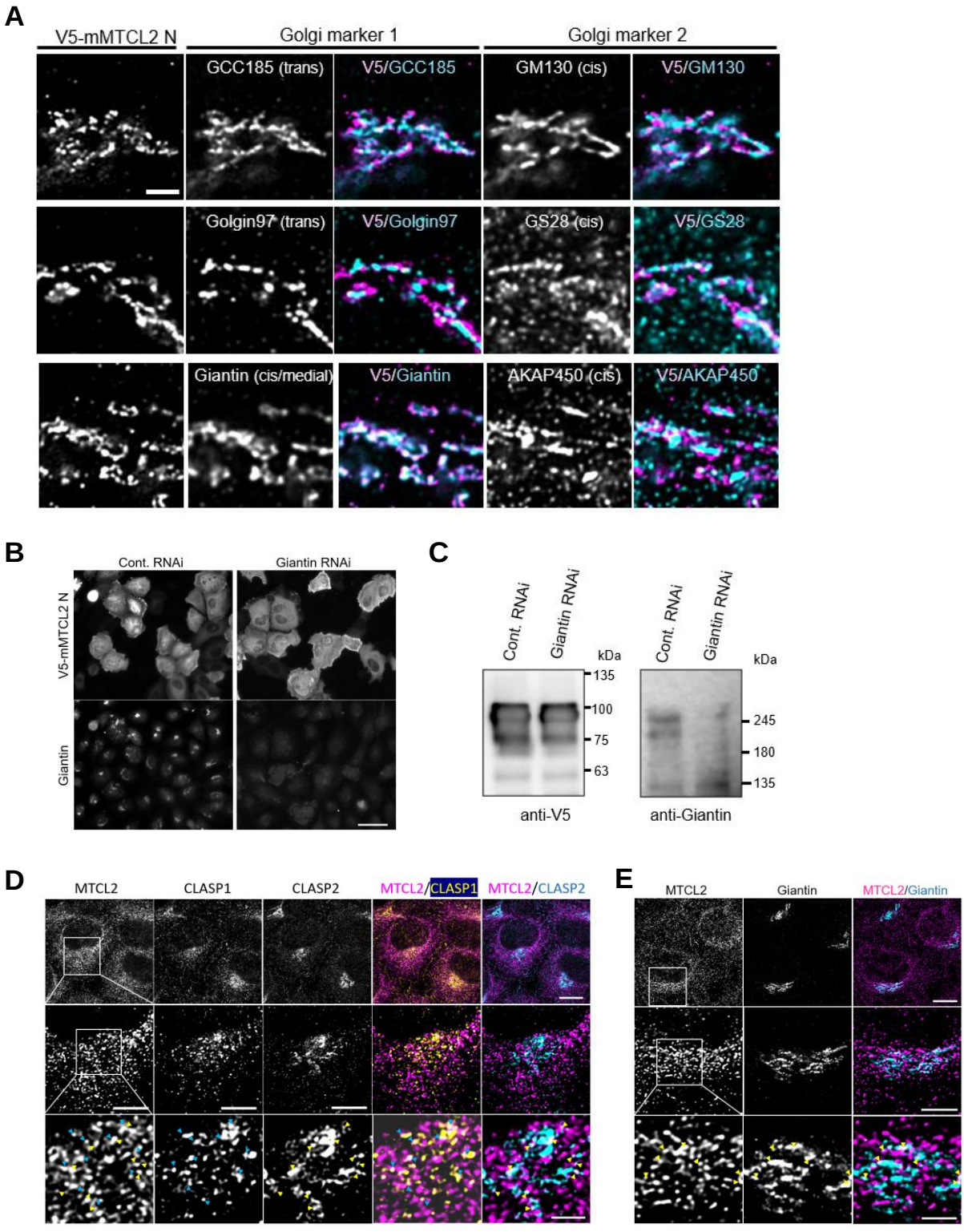

Fig. S7. Giantin is involved in the Golgi association of the MTCL2 N fragment.

(A) Subcellular localization of V5-mMTCL2 N fragment in HeLa-K cells was compared with that of Golgi-resident proteins using super-resolution microscopy. Scale bar: 2μm. Note that the N-terminal fragment of MTCL2 shows colocalization with the cis/medial Golgi protein giantin/GOLGB1 most clearly. The fragment showed distinct localization from cis Golgi marker proteins, suggesting that it is mainly associated with the medial Golgi cisternae. (B) Levels of V5-mMTCL2 N fragment in control and giantin-knockdown cells were compared through immunostaining analysis using the indicated antibodies after paraformaldehyde fixation, which prevented leakage of cytosolic protein during fixation. Scale bar: 50 μm. (C) Levels of V5-mMTCL2 N fragment in control and giantin-knockdown cells were compared through western blotting analysis using total cell extracts. (D and E) Subcellular localization of endogenous MTCL2 in HeLa-K cells was compared with that of CLASPs (D) and giantin (E) using super-resolution microscopy. Boxed regions are serially enlarged in the middle and bottom panels. Arrowheads indicate the regions where each protein shows colocalization with MTCL2. Scale bars: 10 μm (top), 5 μm (middle), and 2 μm (bottom).

Supplementary Figure S8 "Blot Transparency"

Fig.1B

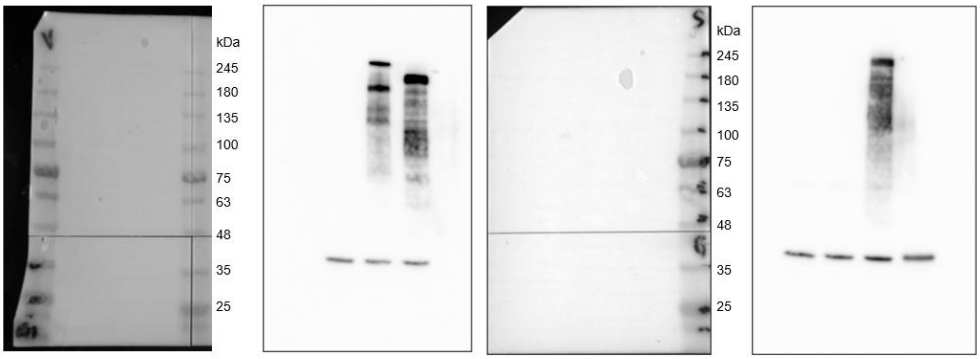

Fig.1C

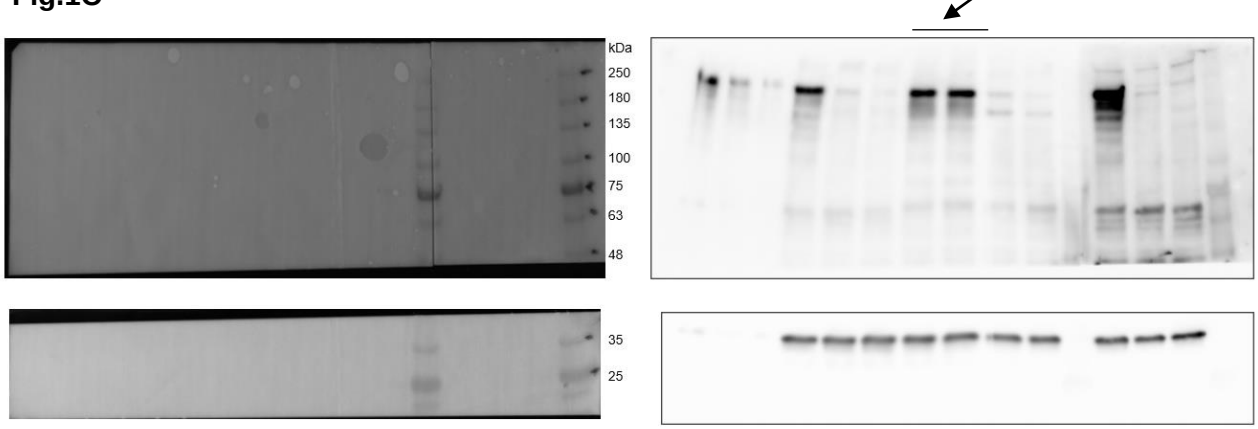

Fig.1D

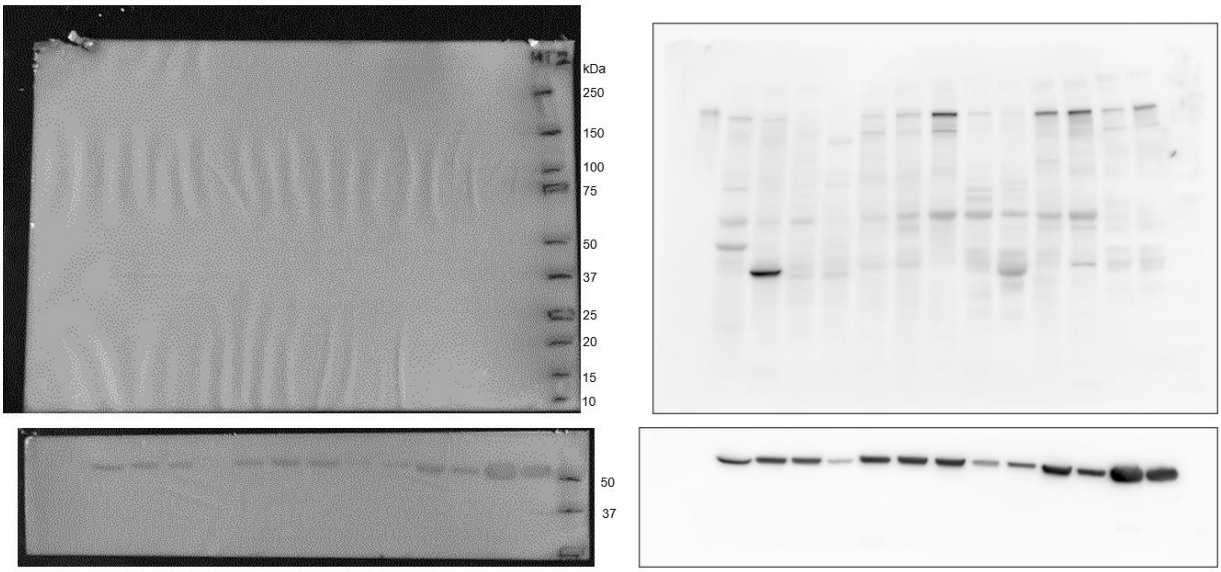

Fig.3C

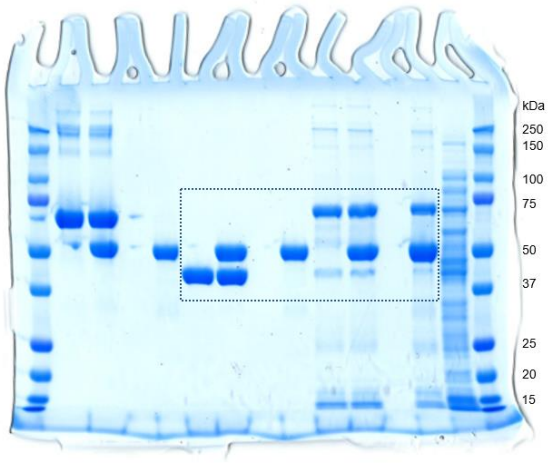

Fig.3E

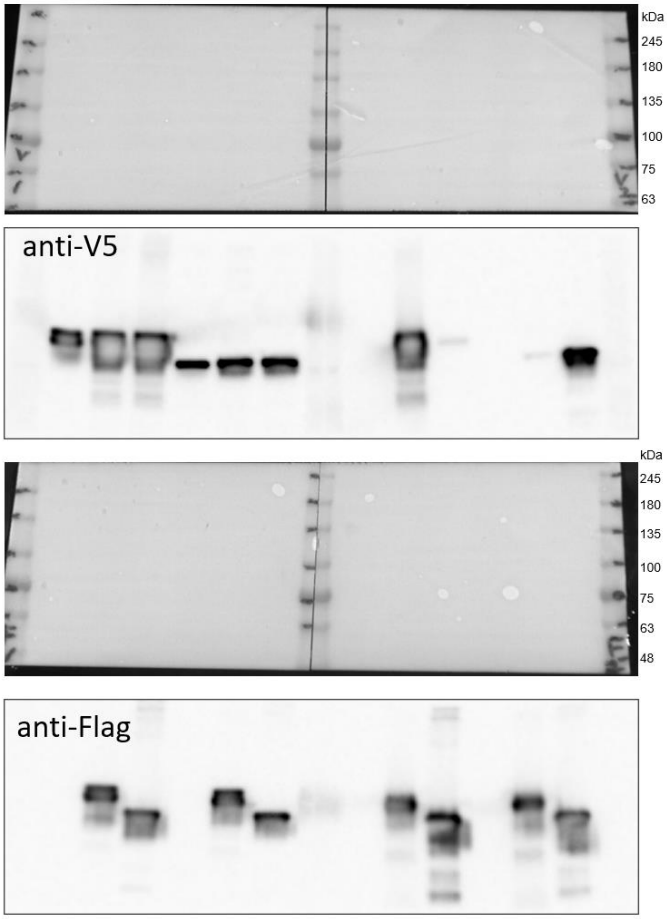

Fig.8B

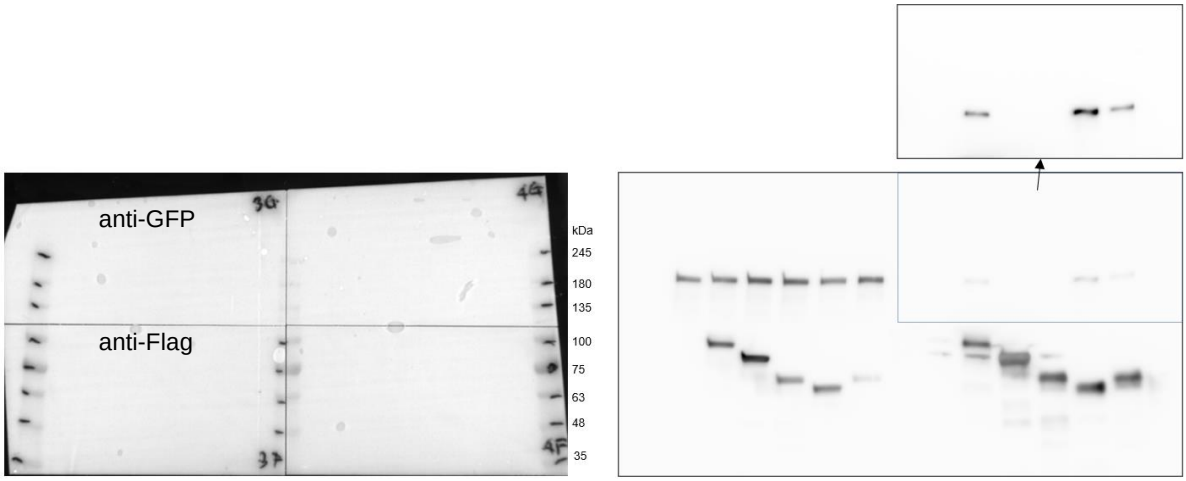

Supplementary Fig.S3C

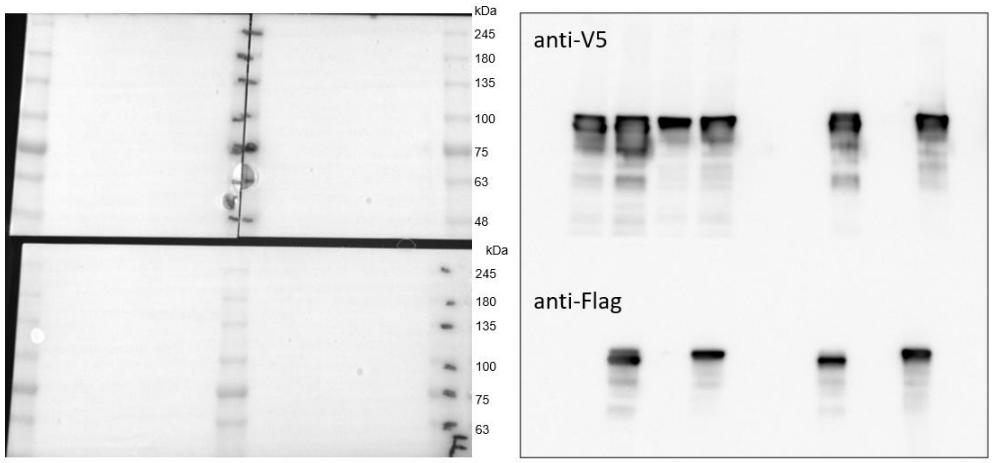

Supplementary Fig.S7C

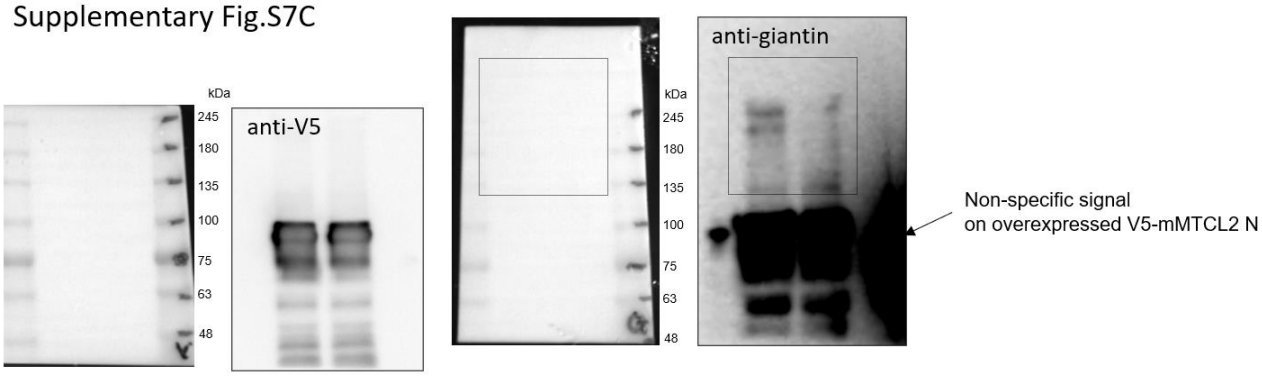

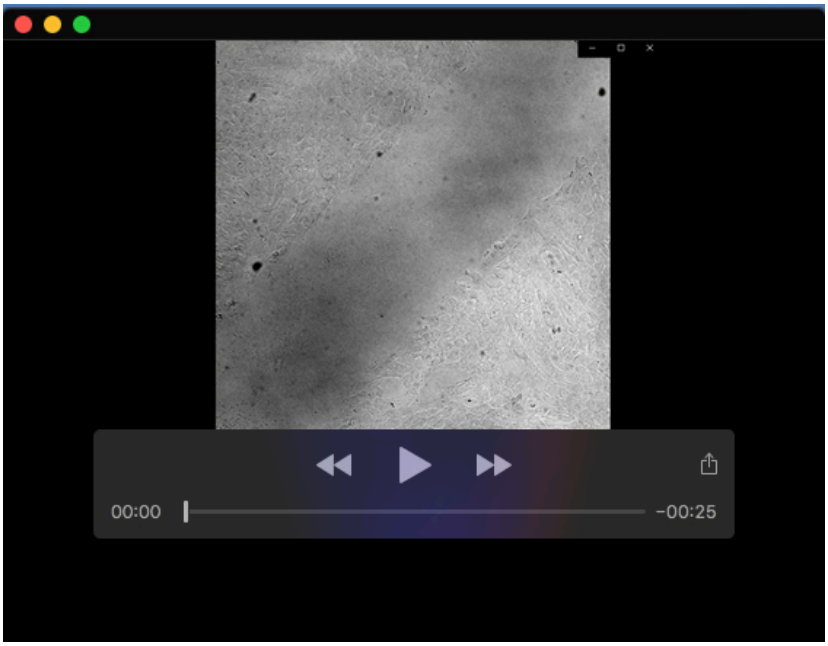

Movie 1. Wound healing of RPE1 cells subjected to control knockdown. Differential interference contrast images of cells were taken every 10 min for 440 min. The video speed is 6 fps. Representative frames of this movie are shown in Fig. 7B.

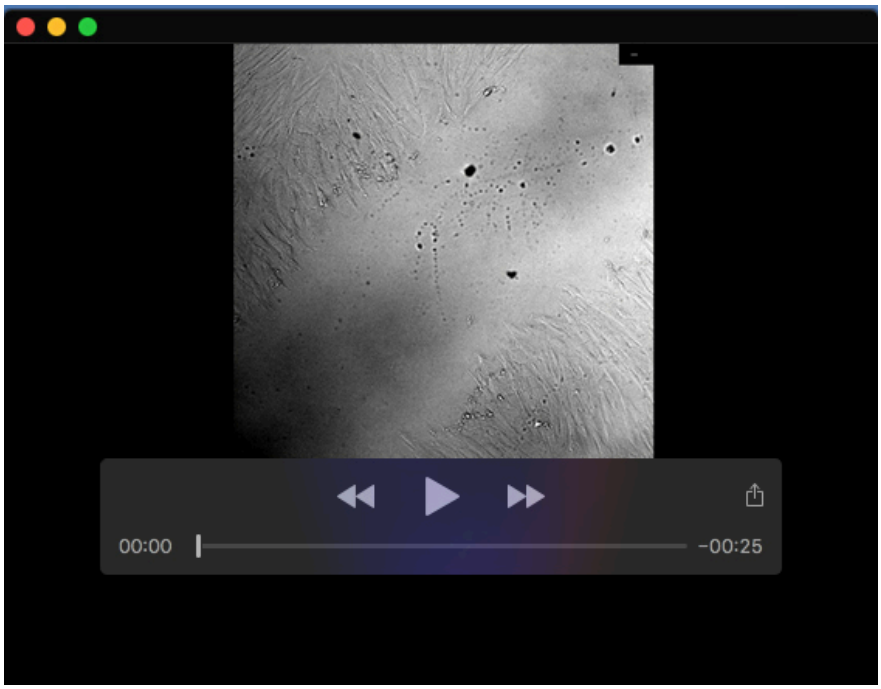

Movie 2. Wound healing of RPE1 cells subjected to MTCL2 knockdown. Data were collected as described in the supplementary material Movie 1 legend. Representative frames of this movie are shown in Fig. 7B.